A Physical Approach to Morphogenesis

MAXIME TORTORA

École Normale Supérieure de Cachan
mtortora@ens-cachan.com

Supervisor: CYPRIEN GAY*
Collaborator: FRANÇOIS MOLINO†

Abstract

We hereby describe a 2D-mechanical model for cell aggregates based on a simple physical analogy to closed-cell foams. The dynamics are ruled by a combination of geometrical parameters and surface tensions, similarly to "classical" soft-matter objects. The active properties of living tissues are recovered through an original cell cortex rheological law. An analytically-solvable model to quantify two-cell adhesion processes is also proposed. A rapidly-converging linear resolution method is finally introduced to compute the coupled evolutions of the macroscopic variables involved. The qualitative results obtained in a few simple geometries are found to be consistent with both observations and experimental data.

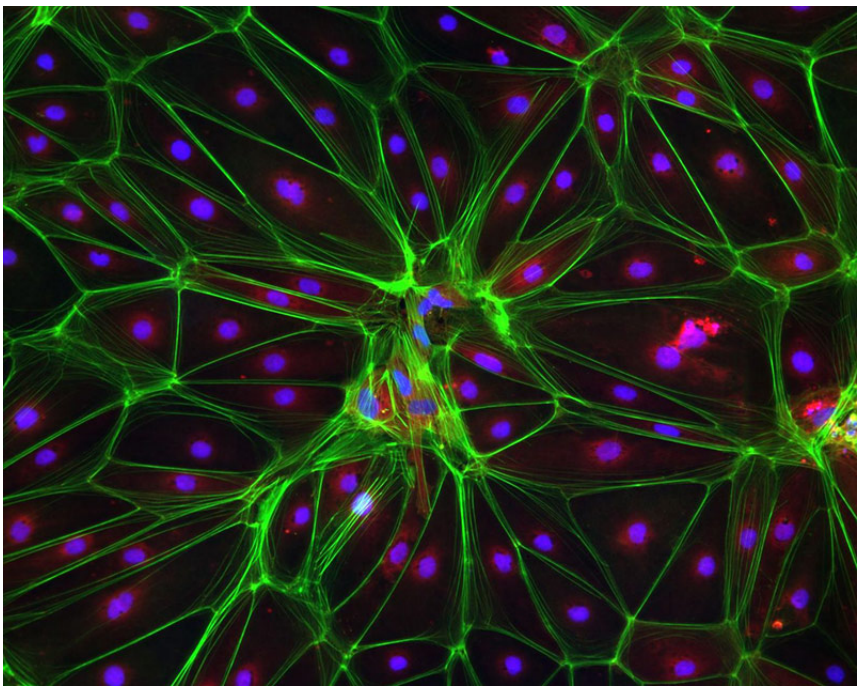

Figure 1: *Human stem cells aggregate - membranes and nuclei (©A. Balachandran).*

*Laboratoire Matière et Systèmes Complexes, Paris 7
†Institut de Génomique Fonctionelle et Laboratoire Charles Coulomb, Montpellier 2

Contents

I Introduction **3**
1 Tissue mechanics in a nutshell . . . 3
2 Presentation of the model . . . 3

II Mechanical Considerations **4**
1 Passive properties of cell aggregates and analogy to foams . . . 4
1.a Plateau's laws . . . *5*
1.b Young-Laplace equation . . . *6*
2 Recovery of the active cell properties . . . 7
2.a J. Étienne's cortex rheology . . . *7*
2.b Damper cortex rheology . . . *9*
2.c Cadherins and cell-cell adhesion model . . . *10*
3 Resolution method . . . 13
3.a Mathematical assumptions . . . *13*
3.b Description of the algorithm . . . *14*

III Application to symmetrical configurations **15**
1 Single-cell between two plates . . . 15
1.a Geometrical and mechanical parametrisation . . . *15*
1.b Set of equations . . . *16*
1.c Results . . . *18*
2 Chain of identical cells . . . 20
3 Rectangular-lattice tissue . . . 21

IV General Geometry **22**
1 Parametrisation . . . 22
2 Degrees of freedom . . . 23

V Conclusion **24**

Appendices

Appendix A Complements on geometry . . . 26

Appendix B General resolution of a cell-cell contact . . . 28

Appendix C Cadherin curvature derivation . . . 30

Appendix D Cadherin curvature integral . . . 33

I. INTRODUCTION

MORPHOGENESIS, literally "creation of shape", refers to a set of biological processes through which a living organism may develop and retain its form. It encompasses a wide variety of mechanisms and scales, from the formation of multicellular arrays and tissues to the higher order assembly of tissues into organs and whole organisms. Morphogenesis is traditionally considered an integral part of developmental biology, emphasising a genetics-based approach to tissue formation. However, mechanical forces also play a dominant role in determining tissue shape and properties both at the intra- and extracellular levels. It has been shown that external stress may even alter the gene expression of cells, thus influencing cell fate determination [12]. This complex set of response mechanisms is known as **mechanotransduction**.

1. Tissue mechanics in a nutshell

Biologists of the early *Entwicklungsmechnik* ("developmental mechanics") movement noted the influence of external forces on embryo development as early as 1888 [18]. However, the limited experimental data available at the time did not allow for a rigorous reductionistic interpretation of the observed tissue dynamics [13]. The relationship between morphogenesis and mechanics has remained an active study field throughout the 20th century, e.g. in the seminal works of Holtfreter and Steinberg in the 50s [11], and has garnered increasing scientific interest over the last few years.

The reasons behind this renewed scrutiny are twofold. The first lies with the recent development of high-resolution image acquisition methods and nanoscopic experimental devices, allowing for the first *in vivo* measurements of mechanical forces in cellular tissues to be made [4]. The second arises from the emergence of regenerative medicine and tissue engineering as promising research fields, striving to understand stem-cell differentiation processes within the framework of morphogenesis to bolster living tissue regeneration, and even allow for *in vitro* growth of entire organs [17]. Both innovations have emphasised the need for a deeper physical understanding of the mechanical factors involved in tissue development; the extent of the modern physical literature on the subject (see [9] for a short review) mirrors that of the medical applications at stake.

2. Presentation of the model

Forces within living cells are typically generated by a family of biological molecular motors[1] in the cytoplasm known as myosins, bound to the surrounding cell cortex[2]. They tend to increase the internal cellular stress by continuously pulling pairs of actin filaments together, thus giving rise to the notion of **cell contractility**. This stress may then be propagated throughout the tissue by a network of transmembrane proteins spread on the surface of the cell, acting as mediators of the fundamental **cell adhesion** process behind the formation of cohesive aggregates [9].

Our model aims to phenomenologically reproduce these general properties of living tissues through simple physical arguments borrowed from the field of interface-dominated soft-matter systems. It contrasts with most of the current literature on the subject in that it is purely force-based, allowing for both straightforward calculations and relevant physical interpretation of the dynamics. It also enabled us to undertake a novel approach to cell adhesion processes outside the classical energetics formalism [7], [14]. We shall now present the mechanical assumptions upon which it relies, before detailing its predictions for a few simple symmetrical geometries. The considerations involved in the generalisation to ordinary 2D-tissues will finally be discussed.

[1] Molecular motor: thermally-activated agent performing mechanical work by harnessing local chemical energy.
[2] Cell cortex: network of actin filaments within the cytoskeleton, providing mechanical support for the membrane.

II. Mechanical Considerations

Cellular membranes as dynamical interfaces represent natural vectors through which a cell may generate and respond to forces. They are bound to the cell cortex through a network of ERM[3] proteins, thus linking their properties to the cell's internal stress repartition. Therefore, our working hypothesis states that the cell's mechanical evolution may be decomposed into an interfacial part, corresponding to the contributions of the membrane, and a rheological part, corresponding to the cortex dynamics and summarising cell bulk properties under a single unified response law. We will first proceed to discuss the equations linked to these interfacial dynamics, along with their soft-matter counterparts. We will subsequently introduce two examples of phenomenological rheological laws which may be sampled in the model, and derive a consistent analytic approach to cell adhesion properties within this framework.

1. Passive properties of cell aggregates and analogy to foams

Similarities between tissue mechanics and classical wetting phenomena have long been noted, and may provide simple physical interpretations for several ubiquitous aggregate behaviours [8]. The tendency of single-cells to acquire a spherical shape may be explained in terms of area-minimisation under the effects of a surface tension, similarly to ordinary liquid drops. The dynamics of two-cell adhesion processes (cf. section IV) bears a striking resemblance to that of coalescing gas bubbles. More complex mechanical properties like cell sorting[4] may even be accounted for through simulations of inhomogeneous foams with thermal fluctuations [7].

An illustration of these structural similarities between soap films and living tissues is given in figures 2a and 2b. We will impart in this section a brief description of two sets of physical properties verified by interfacial systems at equilibrium, which will singlehandedly allow for our model to accurately reproduce such foam-like behaviours in 2-dimensional space.

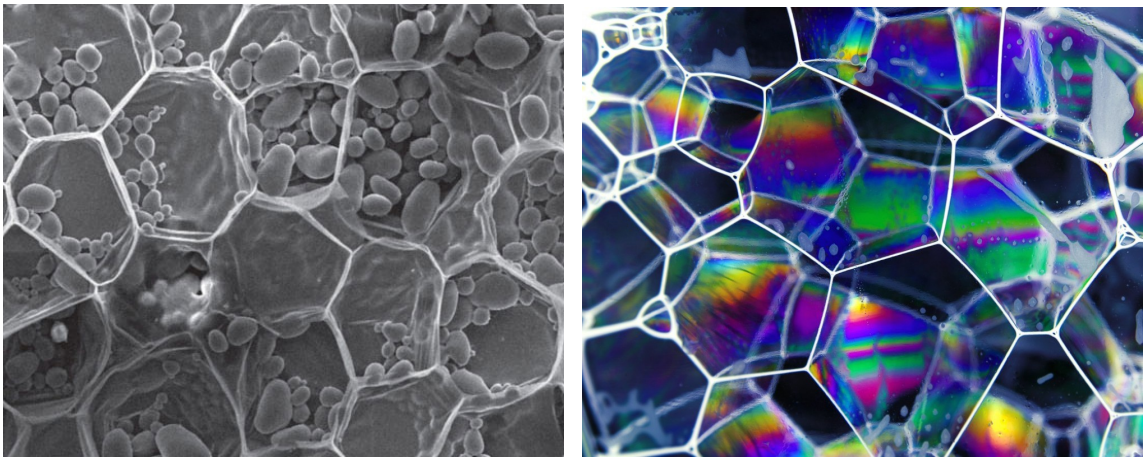

(a) Parenchyma cells arranged in honeycomb-like structure in a potato (©D. Galler, MIT).

(b) Close-up of the local structure of connected soap films in a foam (©S. Ferguson).

Figure 2: *Cell aggregates and soap films.*

[3] ERM: Ezrin, Radixin, Moesin.

[4] Cell sorting: propensity of living cells in aggregates to spontaneously separate and regroup according to their physical and biological properties.

1.a. Plateau's laws

Plateau's laws refer to a set of physical properties characterising the equilibrium configuration of material foams. Based on extensive observation of experimental soap bubbles and their surrounding films, they were originally postulated *circa* 1873 by Belgian physicist J. Plateau. In the case of truly 2-dimensional "dry" foams, holding low water volume fractions, they may be summarised into two simple phenomenological rules [5].

(i) 2D soap bubbles meet in twos along a smooth line called an **edge**, whose curvature is uniform.

(ii) These edges always meet in threes, and do so with an angle of $120°$.

Let us shortly define the vocabulary we shall use in the following.

- For simplicity, we also name **edges** the boundary interfaces with the exterior environment[5].
- Using this definition, we refer to the meeting point of two or more edges as a **vertex** .
- The notions of "volume" and "surface", which we use here for the sake of clarity, should be respectively understood as areas and perimeters in the context of our 2D study.
- In the remainder of this section, we indifferently refer by "cell" to both closed-foam cells and ordinary living cells.

Property (ii) has been mathematically proven to be equivalent to a condition of minimal surface for the foam [19], and thus ensures the stability of the resulting configuration as minimising the film's total energy. An intuitive way to understand this mechanical equilibrium is to consider the simple two-cell system defined figure 3a. We denote by σ the surface tensions of all three interfaces between the two cells and their surroundings, which we assume to be equal. The force-balance equation projected on the horizontal axis of symmetry then reads:

$$\sigma - 2\sigma \cdot \cos\alpha = 0 \tag{1}$$

which bears a unique solution $\alpha = \pi/3$ in $[0, \pi]$, corresponding to a supplementary angle of $120°$.

However, should the values of the three tensions differ, equality (1) no longer holds and the equilibrium contact angles may adapt accordingly. While the uniform stress assumption used to derive (1) is largely true in the case of soap films [5], it has no *a priori* justification within generic living tissues. Therefore, the most general force-balance equation one can write at vertex V reads:

$$\sum_{i \in V} \sigma_i \cdot \overrightarrow{e_i} = \overrightarrow{0} \tag{2}$$

where i indexes the edges leading to vertex V, and $\overrightarrow{e_i}$ denotes the corresponding unitary tangent vector at point V oriented towards the vertex.

Thus, our modelling assumption states that the equilibrium properties of living-cell membranes be qualitatively equivalent to those of the soap films described above, substituting generalised Plateau equilibrium relation (2) for rule (ii). The stresses σ_i, representing generalised surface tensions for the membrane segments, may then be taken as uniform within a given edge; their physical meaning will be further detailed in II.1.b.

In a word, property (i) consequently ensures that cell membranes may be fully described within our model by a collection of circular arcs associated with simple tensile stresses. These curvatures and tensions at each contact zone may subsequently be linked to the overpressures inside the cells through the Young-Laplace relation, which we will now proceed to discuss.

[5] It should be noted that with this wider definition, property (ii) does not formally hold as it only applies within the foam bulk [5]. However, generalised Plateau equilibrium relation (2) is still valid.

1.b. Young-Laplace equation

Derived independently by T. Young and P-S. Laplace in 1806, the Young-Laplace equation provides a strong relation between interfacial tension, curvature and capillary pressure drop across an interface at equilibrium. Imposed by the balance of normal stresses between static fluids meeting along a smooth surface, it should hold across every edge assuming membrane thicknesses to be negligible. Within the framework previously defined in II.1.a, it may be written in canonical form at edge i:

$$\Delta P = C_i \cdot \sigma_i \tag{3}$$

where ΔP denotes the pressure difference[6] between the two cells separated by i (or the cell and the exterior environment, if applicable), and C_i the uniform curvature of edge i.

To obtain (3), it should be noted that we assumed σ_i to bear the meaning of a true effective surface tension, as opposed to the more traditional role of Lagrange multiplier it is usually endowed with in the case of fixed-area membranes. The reason behind this hypothesis is that internal vesicles within the cell have been shown to interact with the membrane at short timescales, either by fusing and providing extra surface at the cost of chemical energy, or by breaking away from it [2]. Therefore, the total membrane area of the cells is free to vary within our model, consistently with our soap film analogy.

Thus, relations (2) and (3) provide a system of equations verified by both usual foams and living tissues, to be written respectively at every vertex and edge within the aggregate. We will now complete our model with a set of cortex rheological laws, through which we aim to reproduce the main active dynamical properties specific to living cells.

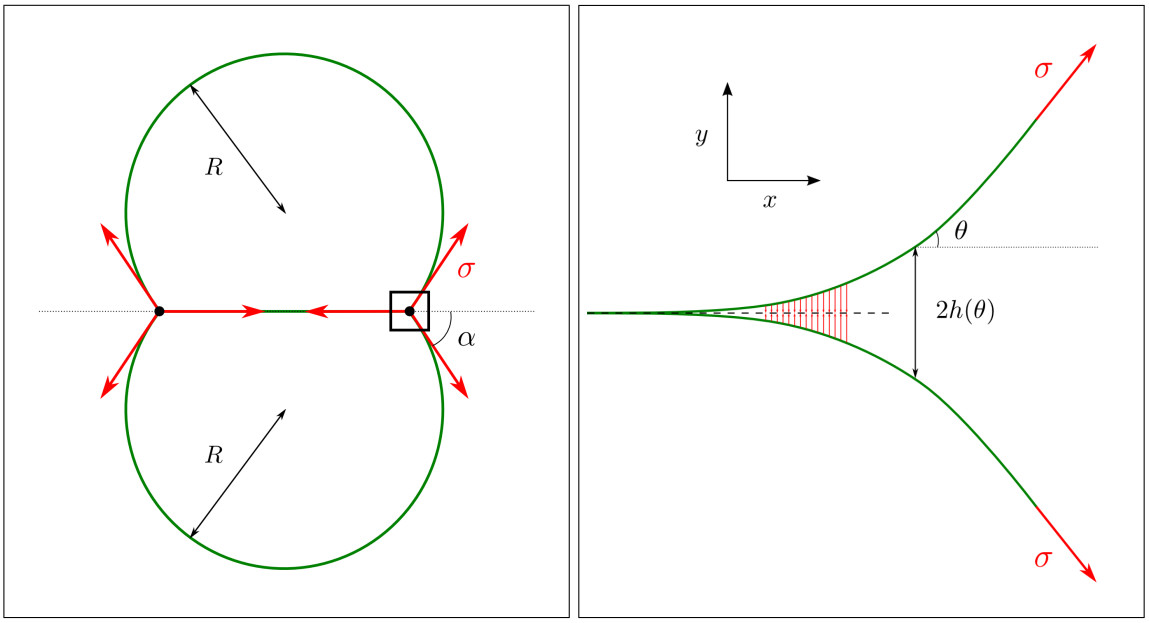

(a) Two-cell Plateau equilibrium. σ denotes the surface tension, assumed equal for all interfaces (uniform stress), and R the macroscopic radius.

(b) Close-up of the black square figure (3a). θ denotes the running angle, and $h(\theta)$ the distance separating the membranes.

Figure 3: *Symmetric two-cell contact zone and geometrical parametrisation.*

[6] Some considerations linked to the respective signs of ΔP and C_i will be mentioned in III.1 and IV.1.

2. Recovery of the active cell properties

For consistency with the equilibrium foam analogies detailed in subsection II.1, we will restrict our study to quasi-static dynamics so that Plateau and Laplace laws hold at all times. Consequently, our previous considerations provide us with a system of "static" equations constraining the evolution of our cell[7] aggregate throughout the simulation. Within this framework, we now seek to describe the processes through which cells may generate and adapt to mechanical stress by means of a simple qualitative law, which will govern the dynamical behaviour of our system.

We will thus attempt to account for the active contractility and adhesion properties of living tissues through a purely physical approach involving a minimal number of parameters, linked to the microscopic state of the cells. We will consider in the following a membrane wall edge as defined in II.1.a, tightly bound to the local cortex within the cell, and assume its stress and strain conditions to accurately match those of the cortex underneath. Therefore, the constitutive equation we pursue may be fully determined by the rheological behaviour of the cell cortex. We will now proceed to discuss two simple phenomenological examples of such rheological models, adapted from the literature.

2.a. J. Étienne's cortex rheology

The main rheological law we have used in our simulations is borrowed from J. Étienne *et al.* [6], and assumes cortex dynamical behaviours may be described by a combination of visco-elastic and active contractile properties. Its diagrammatical representation is given figure 4:

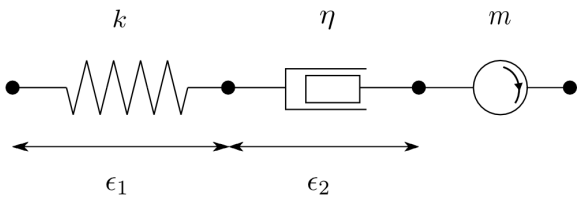

Figure 4: *J. Étienne's cell cortex rheology model.*

The spring, of stiffness k, accounts for the short-time elasticity of the membrane. The damper, of viscosity coefficient η, represents the ability of the cross-links[8] tying the actin filaments together to unbind under applied stress, allowing the actin meshwork to relax and extend at longer times. The motor, of constant velocity m, models the effect of the molecular motors continuously pulling on the actin filaments within the cortex.

It is easy to derive the constitutive equation of such a material by noticing that two elements in series must convey the same stress:

$$\sigma(t) = k \cdot \epsilon_1(t) = \eta \cdot \dot{\epsilon_2}(t) \tag{4}$$

where $\dot{X}$ denotes the derivative of X with respect to time. The strain $\epsilon(t)$ of the membrane element is defined as:

$$\dot{\epsilon}(t) = \frac{\dot{L}(t)}{L(t)} \tag{5}$$

[7] From here on, "cell" should be understood as referring to ordinary living cells.
[8] See figure 6 for a sketch of these cross-links.

where $L(t)$ refers to the total curvilinear length of the membrane wall edge. In the case of the system drawn figure 4, it must verify:

$$\dot{\epsilon}(t) = \dot{\epsilon_1}(t) + \dot{\epsilon_2}(t) - m \tag{6}$$

Plugging relation (4) into (6) immediately yields the governing equation:

$$\dot{\epsilon}(t) = \frac{\dot{\sigma}(t)}{k} + \frac{\sigma(t)}{\eta} - m \tag{7}$$

which relates membrane wall stress and strain within our model. Let us now discuss the behaviour of (7) in two simple situations.

- If the membrane is submitted to a constant stress σ_0, (7) becomes:

  $$\dot{\epsilon}(t) = \frac{\sigma_0}{\eta} - m$$

  and the membrane wall grows with a constant strain rate given by a competition between the unbinding of the actin cross-links, which tends to stretch it proportionally to σ_0, and the molecular motors, which tend to shrink it.
- If the membrane is firmly clamped, $\epsilon = 0$ and the resolution of (7) yields:

  $$\sigma(t) = \sigma_0 \cdot \exp\left(-\frac{k}{\eta} \cdot t\right) + \eta m \cdot \left[1 - \exp\left(-\frac{k}{\eta} \cdot t\right)\right]$$

  dictating that membrane stress equilibrate to $\sigma_{st} = \eta m$ after a characteristic time $\tau = \eta/k$.

In the case where the membrane is submitted to a known strain pattern $\dot{\epsilon_{op}}(t)$, the general solution to (7) reads:

$$\sigma(t) = \sigma_0 \cdot e^{-t/\tau} + k \int_{t'=0}^{t} dt' \cdot e^{-(t-t')/\tau} \cdot [\dot{\epsilon_{op}}(t') + m] \tag{8}$$

An important particular case of (8) may be obtained by considering harmonic imposed strain $\epsilon_{op}(t) = \epsilon_0 e^{i\omega t}$:

$$\sigma(t) = \sigma_0 \cdot e^{-t/\tau} + \sigma_{st} \cdot \left(1 - e^{-t/\tau}\right) + \epsilon_0 \cdot \frac{i\omega\eta}{1 + i\omega\tau} \cdot \left(e^{i\omega t} - e^{-t/\tau}\right) \tag{9}$$

Therefore, after a transient response of duration τ, the system reaches a linear oscillation regime with offset σ_{st}. We will make further use of this property for numerical harmonic analysis in the case of simple geometries, section III.

In the following, we choose to rescale times by $\tau = \eta/k$ in the constitutive equation:

$$\frac{k}{\eta} \cdot \dot{\epsilon} = \frac{1}{\eta} \cdot (\dot{\sigma} + \sigma) - m$$

and rescale stresses by k to obtain the dimensionless form of (7):

$$\boxed{\dot{\epsilon} = \dot{\overline{\sigma}} + \overline{\sigma} - \overline{m}} \tag{10}$$

with $\overline{\sigma} = \sigma/k$ and $\overline{m} = m\tau$. Note that we have here assumed cortical parameters k, η and m to remain constant through the simulation; should they be allowed to vary, the more general form of the constitutional equation reads:

$$\dot{\epsilon} = \frac{\dot{\sigma}}{k} + \left(\frac{1}{\eta} - \frac{\dot{k}}{k^2}\right) \cdot \sigma - m \tag{11}$$

2.b. Damper cortex rheology

An important shortcoming of the J. Étienne rheology is that it fails to introduce a timescale for the dynamics of strain ϵ, though it does provide a time constant τ in the evolution of stress σ. Consequently, membrane strain response to an abrupt change in stress, caused for instance by a sudden compression of the cell[9], may be discontinuous in time. To work around this limitation, one may consider a slightly more complex rheological law, defined diagrammatically figure 5:

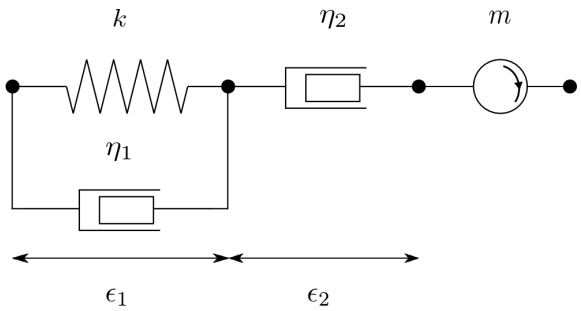

Figure 5: *"Damper" cortex rheological model.*

With the addition of a damper in derivation of the spring, the stress within the membrane wall now reads:

$$\sigma(t) = \eta_1 \cdot \dot{\epsilon_1}(t) + k \cdot \epsilon_1(t) = \eta_2 \cdot \dot{\epsilon_2}(t) \tag{12}$$

Using (6) again, and noting that m does not depend on time:

$$\dot{\sigma} = \eta_1 \cdot (\ddot{\epsilon} - \ddot{\epsilon_2}) + k \cdot (\dot{\epsilon} - \dot{\epsilon_2} + m)$$

Differentiating (12) provides the additional relation:

$$\ddot{\epsilon_2}(t) = \frac{\dot{\sigma}(t)}{\eta_2} \tag{13}$$

Substituting (12) and (13) for $\dot{\epsilon_2}$ and $\ddot{\epsilon_2}$ finally yields:

$$\frac{\eta_1}{k} \cdot \ddot{\epsilon} + \dot{\epsilon} = \left(1 + \frac{\eta_1}{\eta_2}\right) \cdot \frac{\dot{\sigma}}{k} + \frac{\sigma}{\eta_2} - m \tag{14}$$

which defines timescale $\tau_\epsilon = \eta_1/k$ for the strain.

Intuitively, this time constant corresponds to the relaxation time of the first damper and spring in derivation figure 5, which ensures that the total length of the drawn system may not vary abruptly. Such discontinuous behaviours were however allowed by the simple spring in figure 4, which may stretch instantaneously under the effect of fluctuating stress.

We have thus introduced two governing laws to account for the main mechanical properties of the cell bulk and membrane. In the scope of this report, we will restrict ourselves to the case of dimensionless constitutive equation (10), assuming all rheological parameters to be independent of time, and drop the overbar notation for simplicity. We now wish to complete our description of the active properties of living tissues with a simplified model for cell-cell adhesion processes, which we derive hereafter in the case of a two-cell contact zone.

[9] As performed experimentally by C. Wilhem at MSC.

2.c. *Cadherins and cell-cell adhesion model*

General properties of cell adhesion. Cell adhesion molecules regroup several families of transmembrane proteins spread on the surface of the cell which may locally interact with their counterparts located in nearby cells or within the extracellular matrix, through a variety of chemical mechanisms [3]. In the following, we will restrict our study to the family known as **cadherins**[10], assuming the adhesive behaviours of the other protein sets to be qualitatively similar.

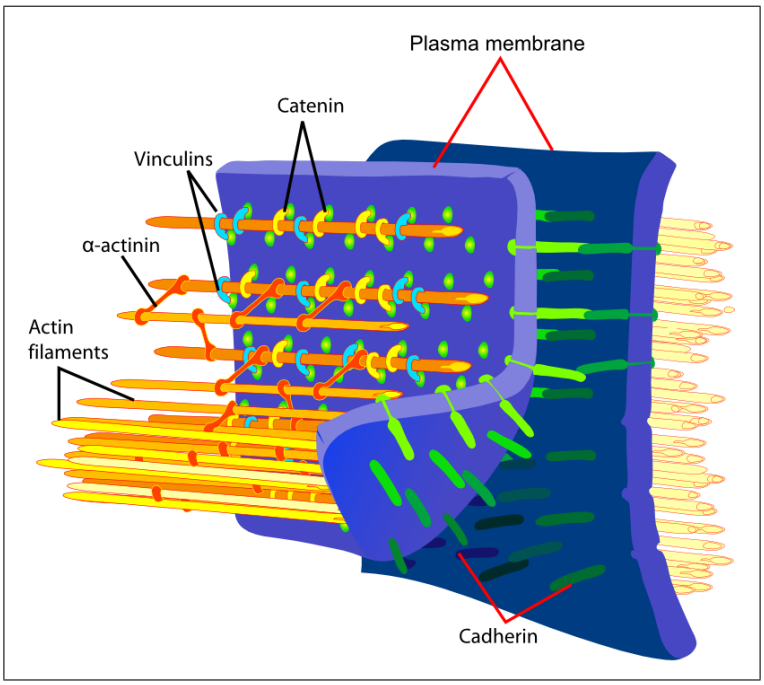

Figure 6: *Cadherins, cell cortex and actinin cross-links (©M. Ruiz).*

As illustrated in figure 6, cadherins are linked to the actin filaments within the cortex via several cytoplasmic proteins, though the exact mechanisms underlying these bonds are still under investigation [15]. Therefore, cadherin-mediated adhesion appears to be naturally related to the cortex rheological formalism detailed in the previous section.

Within this framework, let us consider the two-cell border zone described figure 3b. Locally, the free cadherins located beyond the contact section are likely to bind with each other, provided the membranes are close enough. In the process, they extend the length of the adhering region by further pulling the two membranes together. Therefore, in the reference frame of the membranes in contact, cadherins induce a cortex circulation directed towards the adhering zone, cf. figure 7a.

Let us denote by v_{ca} the local velocity of this cortex flow, and define by L_c the curvilinear length of the membrane segments in contact. The time evolution of L_c must then be such that:

$$\dot{L_c}(t) = \dot{\epsilon_c}(t) \cdot L_c(t) + v_{\mathrm{ca}}(t) \tag{15}$$

where we have modified (5) to account for the extra membrane length being "pumped" by the cadherins into the contact zone. Similarly, the length L of the free membrane edges must verify:

$$\dot{L}(t) = \dot{\epsilon}(t) \cdot L(t) - v_{\mathrm{ca}}(t) \tag{16}$$

[10] Short for Calcium-dependent adhesion.

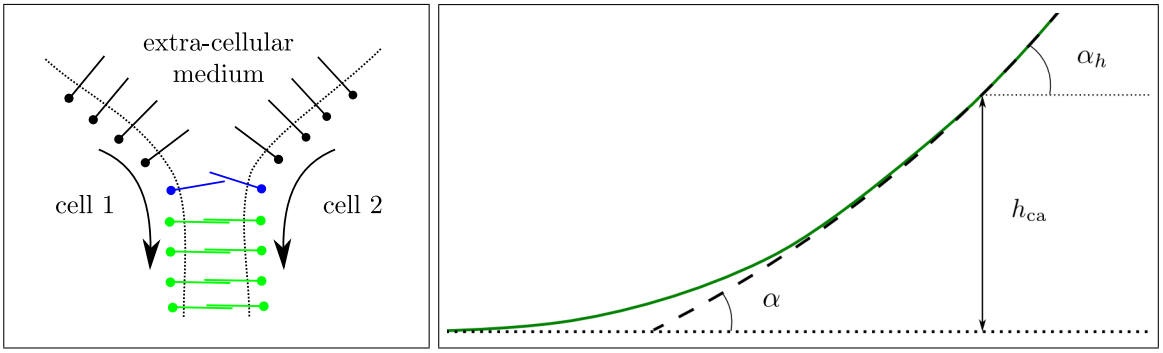

(a) Contact zone dynamics and cadherin-induced cortical flows (©V. Boudara).

(b) Definition of angles α, α_h and cadherin interaction range h_{ca}. The dashed black contour represents the idealised circular free membrane, neglecting the microscopic adhesion zone.

Figure 7: *Cadherins and local adhesion zone, in the case of a symmetric two-cell contact.*

Brief presentation of the model. We now wish to derive the evolution of flow velocity v_{ca}, and compute its dependency to the relevant macroscopic variables within our model. In that aim, one has to provide a thorough mechanical description of the local area beyond the contact point, defined in figure 3b, which governs the dynamics of cell adhesion. We only explicit here the outline of this analysis, and refer the reader to appendix C for the detailed calculations.

The membrane profile along the microscopic cadherin adhesion zone, denoted by red stripes in figure 3b, may be parametrised by curvilinear abscissa s and angle $\theta(s)$ with respect to the contact line. Let us provide the following definitions:

- Using the notations of figure 3, we denote by $C = 1/R$ and σ the macroscopic curvature and stress of the free spherical membrane segments, far from the adhesion zone.
- We define by σ_μ and C_μ the local microscopic stress and curvature in the adhesion zone, respectively.
- We assume the contribution of the membrane bending modulus to be negligible.
- We assume the cadherins to have a maximum range of interaction h_{ca}, so that two membrane elements belonging to different cells may only "see" each other if they are separated with a distance $h \leq h_{\mathrm{ca}}$.
- We denote by α_h the value of θ for which $h(\theta) = h_{\mathrm{ca}}$.
- We define c as the average cadherin concentration within the contact zone, and F_0 as the average force exerted by a single cadherin.
- We finally refer to the overpressure within the cell by P.

One may then prove the following relations:

$$C_\mu(\theta) = C \cdot \frac{(1+\psi\cos\theta)^2}{1+\psi\cos\alpha_h} \tag{17}$$

$$\sigma_\mu(\theta) = \sigma \cdot \frac{1+\psi\cos\alpha_h}{1+\psi\cos\theta} \tag{18}$$

where we have defined:

$$\psi = \frac{cF_0}{P} \tag{19}$$

Note that because of the local forces exerted by the cadherins, stress σ_μ and curvature C_μ are not uniform within the adhesion zone, unlike their macroscopic counterparts. In the absence of

cadherins, $\psi = 0$ and one recovers from (17) and (18) the macroscopic membrane properties. One may further derive the following relations for c and α_h:

$$c = \frac{\sigma}{h_{\text{ca}} F_0} \cdot (1 - \cos\alpha) \tag{20}$$

$$\cos\alpha_h = \cos\alpha - \frac{h_{\text{ca}}}{R} \tag{21}$$

Relation (21) may be intuitively understood by considering figure 7b: macroscopic angle α is defined by neglecting the microscopic adhesion zone, and by assuming the macroscopic free membrane of radius R abruptly intersects the contact line at a sharp angle. More realistically, the local cadherin interactions impose a smoother transition between free membranes and membranes in contact, and one only recovers the macroscopic properties of the free edges upon leaving the adhesion area, at angle $\alpha_h > \alpha$.

The total number N of interacting cadherins in the zone is then given by:

$$N = c \cdot \delta s \tag{22}$$

with δs the microscopic membrane length within which cadherins are close enough to interact:

$$\delta s = \int_0^{\delta s} ds = \int_0^{\alpha_h} \frac{d\theta}{C_\mu(\theta)} \tag{23}$$

Integral (23), computed analytically in appendix D, is given by (125). The total force F generated by the cadherins perpendicularly to the contact line reads:

$$F = N \cdot F_0 = c \cdot \delta s \cdot F_0 \tag{24}$$

The effective force F_{eff} exerted on the membrane segment in the adhesion zone may then be obtained by subtracting the component of macroscopic stress σ normal to the contact line, which antagonistically tends to tear the two cells apart:

$$F_{\text{eff}} = c \cdot \delta s \cdot F_0 - \sigma \cdot \sin\alpha \tag{25}$$

Substituting (20) for c:

$$F_{\text{eff}} = \frac{\sigma}{h_{\text{ca}}} \cdot (1 - \cos\alpha) \cdot \delta s(\psi, \alpha_h) - \sigma \cdot \sin\alpha \tag{26}$$

which only depends on macroscopic variables σ, α, P and R computed within the model, and on microscopic constants h_{ca} and F_0. Finally, one may simply approximate the induced cortex velocity to be proportional to this local adhesion force borne by the membrane:

$$\boxed{v_{\text{ca}} = \lambda \cdot \left[\frac{\sigma}{h_{\text{ca}}} \cdot (1 - \cos\alpha) \cdot \delta s(\psi, \alpha_h) - \sigma \cdot \sin\alpha \right]} \tag{27}$$

with λ a scaling constant to be chosen consistently with the size of the studied cells. It should be noted that this proportionality assumption is not strictly necessary, and one may directly infer the velocity of the contact point from length δs and concentration c via a few additional mechanical considerations. However, due to time constraints, we will not discuss these subtleties in the scope of this report; they will likely be the subject of an article to be written in the months to come.
Let us now shortly present the resolution method we developed to solve the complex system of coupled equations derived in the previous subsections.

3. Resolution method

3.a. Mathematical assumptions

Let us define a set of variables $\{x_i(t)\}_{1\leq i\leq n}$ fully describing the cell aggregate within our model. Let $(E_j)_{1\leq j\leq m}$ be the set of physical equations constraining the evolutions of the (x_i). We assume that for quasi-static dynamics, the (E_j) may be given under the form of the following system[11]:

- a set of coupled equations (e.g., Laplace and Plateau relations), indexed by:

$$f_k\left(x_1, x_2, \ldots, x_n\right) = a_k(t) \qquad \forall k \in [\![1, p]\!] \tag{28}$$

- a set of ordinary first-order differential equations (e.g., rheological laws), indexed by:

$$g_l\left(\dot{x_1}, \ldots \dot{x_n}, x_1, \ldots, x_n\right) = b_l(t) \qquad \forall l \in [\![1, q]\!] \tag{29}$$

with p and q such that $m = p + q$. We further assume the f_k to be differentiable at all points, and the functions:

$$(\dot{x_1}, \ldots, \dot{x_n}) \to g_l\left(\dot{x_1}, \ldots, \dot{x_n}, x_1, \ldots, x_n\right)$$

to be linear $\forall\left(x_1, \ldots, x_n\right)$ and l.

Under these hypotheses, equation (29) may be written in the form:

$$^tA_l(X) \cdot \dot{X} = c_l(X, t) \tag{30}$$

with $X = (x_1, \ldots, x_n)$ and $A_l(X)$ the n dimensional vector holding the linear coefficients of the $\dot{x_i}$ in g_l. Furthermore, (28) imposes the following equality for the f_k differentials:

$$\frac{df_k}{dt}\left(x_1, \ldots, x_n\right) = \dot{a_k}(t) = \sum_{i=1}^{n} \frac{\partial f_k}{\partial x_i} \cdot \dot{x_i}$$

Thus, equation (28) may be equivalently written as follows in differential form:

$$^tB_k(X) \cdot \dot{X} = \dot{a_k}(t) \tag{31}$$

with B_k the n dimensional vector defined by:

$$B_k(X) = \left\{ \frac{\partial f_k}{\partial x_i}\left(x_1, \ldots, x_n\right) \right\}_{1\leq i\leq n}$$

Combining (30) and (31), the constraints $(E_j)_{1\leq j\leq m}$ may finally be written in the form:

$$M(X) \cdot \dot{X} = C(X) \tag{32}$$

with $M(X)$ the $m \times n$ coupling matrix and $C(X)$ the m dimensional vector defined by:

$$M(X) = \quad \left\{^tA_l(X)\right\}_{1\leq l\leq q} \bigcup \left\{^tB_k(X)\right\}_{1\leq k\leq p} \tag{33}$$

$$C(X) = \quad \{c_l(X, t)\}_{1\leq l\leq q} \bigcup \{\dot{a_k}(t)\}_{1\leq k\leq p} \tag{34}$$

From (32), it is clear that one must have:

$$m = n \tag{35}$$

as a necessary condition for the system to be solvable[12]. In that case, and further assuming $M(X)$ to invertible, the vector $\dot{X} = (\dot{x_1}, \ldots, \dot{x_n})$ may be uniquely determined from (32):

$$\boxed{\dot{X} = M(X)^{-1} \cdot C(X)} \tag{36}$$

[11] We will explicitly verify the hypotheses stated in this paragraph in the example presented subsection III.1.

[12] It will be proven in IV.2 that this equality always holds for 2D-tissues.

3.b. Description of the algorithm

Hence, starting from a given configuration $X(t)$ satisfying constraints (E_j) at time t, (36) provides the unique values of the derivatives $\dot{X}(t)$ such that (E_j) still hold at time $t+dt$. Iteratively, all the information pertaining to the coupled evolutions of variables $\{x_i(t)\}$ is thus contained within $M(X)$. Our algorithm's working procedure is then defined recursively as follows.

- The initial state of the system is specifically provided so as to be compatible with the set of constraints (E_j), which depend on the geometry, rheology and parametrisation chosen. This step has to be ensured at $t=0$ either manually, or through a numerical optimisation of the initial variable values with respect to the corresponding system of equations.
- Given a state of the system $X(t)$ satisfying the above conditions, the coupling matrix $M\left[X(t)\right]$ and vector $C\left[X(t)\right]$ may be computed using (33) and (34), respectively.
- The inverse of the coupling matrix $M\left[X(t)\right]^{-1}$ may subsequently be determined numerically, provided M is properly conditioned[13].
- Using (36) along with an Euler discretisation scheme, one may then compute the new values of the system $X(t+dt)$ at the next time step.

This method has the advantage of preserving the system dynamics throughout the calculation, as the evolutions of all variables may be explicitly derived from (36) at each time step. Furthermore, matrix inverses being numerically computable in polynomial time, the algorithm converges significantly faster than most common techniques based on numerical analysis and multivariate optimisation.

However, it is heavily reliant on the fact that coupling matrix $M(X)$ must remain invertible throughout the simulation, and its inverse evaluable with minimal numerical errors. One must therefore choose the working system of equations and variables carefully to avoid singular behaviours of M in the course of the computations. We will now discuss a few such sets of equations used in different geometrical configurations, along with some corresponding predictions of the model.

[13] Some practical considerations relating to the influence of the geometrical parametrisation on matrix conditioning will be discussed in III.1; see [10] for a thorough theoretical introduction to the subject.

III. Application to symmetrical configurations

We here present some concrete results of the model in the context of three simple aggregate geometries. Regrettably, experimental data pertaining to the mechanical properties of single cells and symmetrical tissues is currently scarce, due to the technical difficulties involved in the handling of living cells. We will first fully detail an application of the model to one of the few such single-cell experimental setups currently operated, before shortly mentioning two examples of "crystalline" aggregates as stepping stones towards the generalisation to ordinary tissues.

1. Single-cell between two plates

We here consider an experimental device[14] comprised of a single living cell caught between two parallel micro-plates, as pictured figure 8a. The lower plate, of infinite rigidity, provides the mechanical support for the cell. The upper plate is flexible, with a bending stiffness precisely determined through a preliminary calibration protocol. An optical sensor is used to detect the position of the soft plate extremity in real time, and the evolution of the force exerted by the cell on the plates may thus be dynamically monitored with a precision of the order of the nN.

1.a. Geometrical and mechanical parametrisation

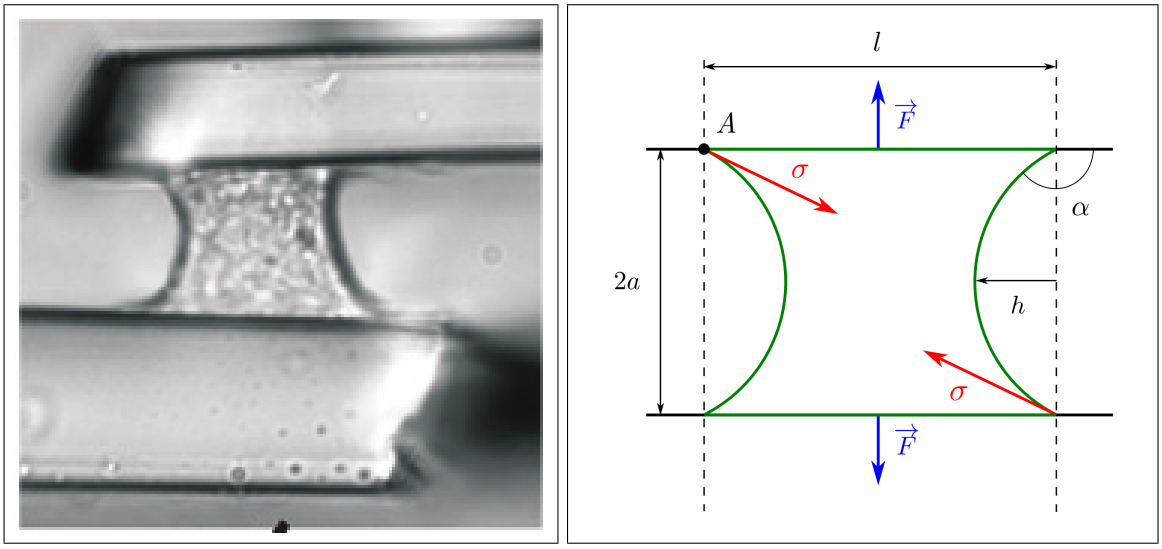

(a) Picture of the experimental device (from [6]). **(b)** Geometrical parametrisation within the model.

Figure 8: *A. Asnacios' single cell experimental setup and simplified 2D-parametrisation.*

The subject cells may spontaneously spread on the plate through the action of a set of trans-membrane proteins referred to as **integrins**. This process, known as cell-substrate adhesion, is assumed[15] to be qualitatively similar to cadherin-mediated cell-cell adhesion as described in II.2.c. The initially spherical cell may thus naturally adopt a shape reminiscent of that of a liquid drop between two plates, as observed figure 8.

[14] The setup described hereafter, developed by Prof. A. Asnacios, may currently be seen at the MSC laboratory.

[15] Note that this assumption is very crude; the dynamics of cell-substrate adhesion involve a complex interplay of local membrane deformations, which is still under investigation [16].

We have here modelled this experiment in dimension 2 by the simple system depicted figure 8b, assuming the cell to be fully symmetrical. Note that as we expect the free membrane curvature to change sign over the course of the simulation, a simple parametrisation via a curvature radius would here result in a poor matrix numerical conditioning. Indeed, going continuously from a spherical geometry to the concave shape drawn figure 8 requires the free membrane wall to reach an intermediary "flat" configuration, which corresponds to an infinite curvature radius.

Let us further emphasise the care that must be taken in the choice of variables for proper conditioning. As an illustration, let us assume the cell volume V_{cell} to be fixed, and choose to parametrise the free membrane wall by curvature C and angle α only. *A priori*, both α and C should remain finite and well-behaved throughout the simulation. However, the volume of the cell may be proven using appendix A to be equal to:

$$V = 2R^2 \cdot \left(\frac{\pi}{2} - \alpha - \frac{\sin 2\alpha}{2}\right) + 2a \cdot l$$

which may be written in the form:

$$C^2 \cdot V_{\text{cell}} = \frac{\pi}{2} - \alpha - \frac{\sin 2\alpha}{2} + 2C^2 \cdot a \cdot l \tag{37}$$

using $C = 1/R$. Differentiating (37) within the resolution framework defined in II.3.b yields:

$$2C\dot{C} \cdot V_{\text{cell}} = -\dot{\alpha} \cdot (1 + \cos 2\alpha) + 2C \cdot (2\dot{C} \cdot al + \dot{a} \cdot C^2 l + \dot{l} \cdot C^2 a) \tag{38}$$

A quick glance at figure 8b indicates that in the flat configuration discussed above, one must have $C = 0$ and $\alpha = \pi/2$. In that case, all the terms in (38) go to 0, and (38) only contributes to coupling matrix M with a line of zeroes which may harm the convergence of matrix inverse M^{-1}. Therefore, one has to resort to a more complex parametrisation involving chord a and height h instead for the proper conditioning of cell volumes in the model.

Consequently, the 9 relevant variables fully determining the state of the cell in our simplified approach are the following:

- semi-chord a of the free membrane wall
- circular height h of the free membrane wall
- contact zone length l
- contact angle α
- curvilinear length L of the free membrane wall
- curvature C of the free membrane wall
- overpressure P within the cell
- stress σ within the free membrane wall
- force F exerted on the plates

1.b. Set of equations

In this framework, we wish to study the evolution of the force $-F$ exerted by the cell on the plate; let us now describe the equations fully describing the cell within our model.

- At short time scales, we assume the membrane to be impermeable to water and the osmotic pressures of the solute to equalise on either side of the membrane. Therefore, we may assume the cell volume to remain constant, which yields a first equation:

$$V_{\text{cell}} = 2a \cdot \left[f_V\left(\frac{\pi}{2} - \alpha\right) \cdot h + l\right] \tag{39}$$

  with f_V the area of the circular contact segment per unit height and chord defined in (61).

- Assuming quasi-static dynamics, for consistency with our equilibrated foam analogy, the Laplace equation reads:
$$P = \sigma \cdot C \tag{40}$$
with C the finite curvature of the free membrane edge on the side.
- Under the same hypothesis, the force balance equation on the upper plate yields:
$$F = -2\sigma \cdot \sin\alpha + P \cdot l \tag{41}$$
where the factor 2 denotes the two free membrane walls, and the signs account for the propensity of cell overpressure P to push the plate upwards.
- The evolution of force F is also imposed by a feedback loop within the experimental setup to be such that (see [1]):
$$\dot{F} = 2k_{\mathrm{pl}} \cdot \dot{a} \tag{42}$$
where k_{pl} denotes the upper plate bending stiffness, and the factor 2 accounts for the fact that a represents the half-distance between the plates.

Note that Plateau equation (2) is not necessary in this very simple geometry, as the membrane in contact is assumed to be tightly bound to the solid plate; it may therefore not convey any stress to the free membrane edge. The equilibrium of vertex A is thus single-handedly ensured by (41).

These physical considerations are supplemented by a set of geometrical constraints, demonstrated in appendix A, which ensure the consistency of our model's dynamics.

- (57) imposes the following relation between angle α, curvature C and curvilinear length L:
$$L \cdot C = \pi - 2\alpha \tag{43}$$
- Relation (55) also dictates that:
$$C \cdot a = \cos\alpha \tag{44}$$
which ensures that $C < 0$ when $\alpha > \pi/2$.
- Equation (58) further yields:
$$h \cdot \cos\left(\frac{\pi - 2\alpha}{4}\right) = a \cdot \sin\left(\frac{\pi - 2\alpha}{4}\right) \tag{45}$$
and one similarly recovers $h < 0$ when $\alpha > \pi/2$.

Finally, two last equations may be obtained by accounting for the rheological and adhesive properties of the cell.

- Relation (16) imposes for the evolution of L:
$$\dot{L} = L \cdot (\dot{\sigma} + \sigma - m) - 2v_{\mathrm{int}} \tag{46}$$
where we have used rheological law (10) in adimensioned units. Adhesion velocity v_{int} is given by (27), and the factor 2 accounts for the two adhesion zones on the upper plate.
- The evolution of contact side length l, clamped to the plate, is then entirely determined by the integrin dynamics at the adhesion zone:
$$\dot{l} = 2v_{\mathrm{int}} \tag{47}$$

Following the resolution procedure defined in II.3, equations (39) to (45) may finally be written in differential form to obtain a coupled system of 9 coupled linear equations (39)–(47), which may be solved at each time step to obtain the derivatives of our 9 variables.

1.c. Results

The typical force curves obtained by our model are found to be in excellent qualitative agreement with the experimental measurements by [1], as illustrated figure 9. The slower evolution observed at the beginning results from the initial configuration of the cell, assumed to be spherical and tangent to the two plates. In that case $l = 0$ and $\alpha = 0$, and neither free membrane stresses nor internal cell overpressure may effectively provide a normal force on the plates. The saturation reached at long times may be understood as an equilibrated competition of the following ingredients.

- Cell contractility, tending to minimise the free membrane length L by forcing the cell into the "flat" configuration.
- Cell adhesion, tending to maximise the spread l of the cell on the plate.
- Plate stiffness k_{pl}, limiting the amount by which the cell may minimise its axial length a in the course of these dynamics with superimposed cell volume V_{cell}.

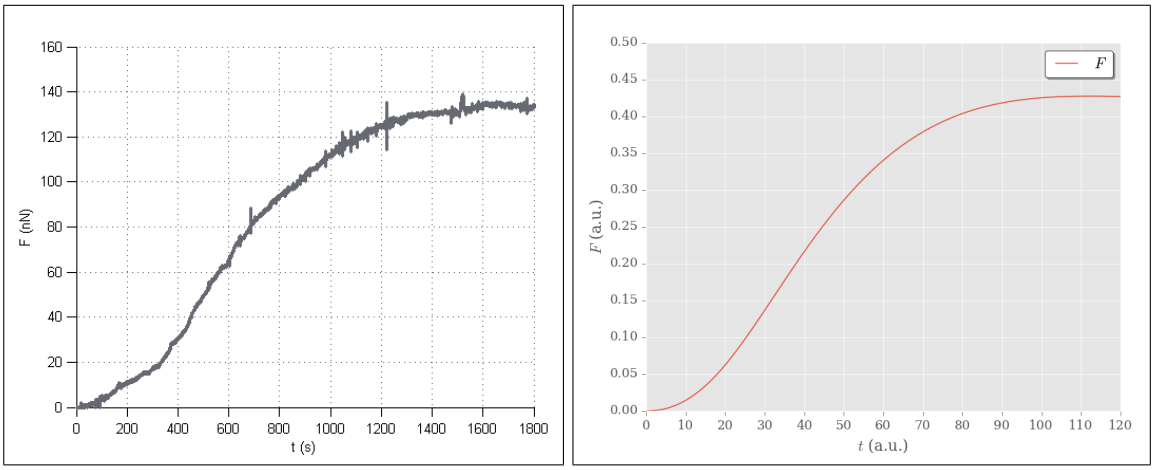

(a) Typical force curve obtained with the experimental setup (from [1]).

(b) Example of a force curve as computed numerically by our model, with $m = 0.1$ and $k_{\mathrm{pl}} = 1$.

Figure 9: *Qualitative comparison of model results and experimental data for the dynamics of force F.*

Because of the adimensioned system of units used and the restriction to 2D considerations, one may not realistically hope to match experimental data in a quantitative way using this simple version of the model; however, these first results appear to be very promising.

It may also be enlightening to compute the harmonic response of the system, so as to assess its behaviour with respect to rheological law (10). In that aim, one has to slightly alter the experimental setup by providing two plates of infinite stiffness, and thus impose a fixed length a for the cell. The distance between the plates may then be precisely modulated in amplitude and frequency to impose an oscillatory regime onto the cell.

To further isolate the effects intrinsic to cell rheology, one may choose to inhibit the action of integrins by altering the preliminary treatment of the micro-plates [1]. In our model, this may be simply achieved by forcing velocity v_{int} and angle α to 0, accounting for the fact that the adhesion point may not convey any stress normally to the plates in this case[16].

[16] Note that in order to ensure the cell always remains in contact with the two oscillating plates in the absence of adhesion, one must first "squash" the cell between the plates to enforce a nonzero contact area. Hence, one has to provide a velocity v_{g} as an additional variable in equations (46) and (47), to account for this geometrically-imposed spreading.

While such a series of experiments was also led by A. Asnacios *et al.*, we were unable to thoroughly exploit their results due to time constraints; we may therefore only report here our own numerical findings, represented figure 10. To qualitatively understand the rheological behaviour of σ over the considered frequency range, one must first notice that as $\alpha = 0$, (43) and (44) impose:

$$L = \pi a$$

Therefore, in the absence of integrins, a is directly proportional to strain ϵ within the free membrane. Thus, using equation (9) in stationary regime:

$$G_\sigma = \frac{\sigma(t)}{a_0 e^{i\omega t}} \propto \frac{\sigma(t)}{\epsilon_0 e^{i\omega t}} \underset{t \gg 1}{\longrightarrow} \frac{i\omega}{1 + i\omega} \tag{48}$$

Consequently, in the low-frequency regime $\omega \ll 1$:

$$G_\sigma \propto i\omega$$

which corresponds to the damper-dominated regime (cf. figure 4). In the high-frequency range, (48) becomes:

$$G_\sigma \propto 1$$

and one recovers a purely elastic membrane behaviour, dominated by the spring.

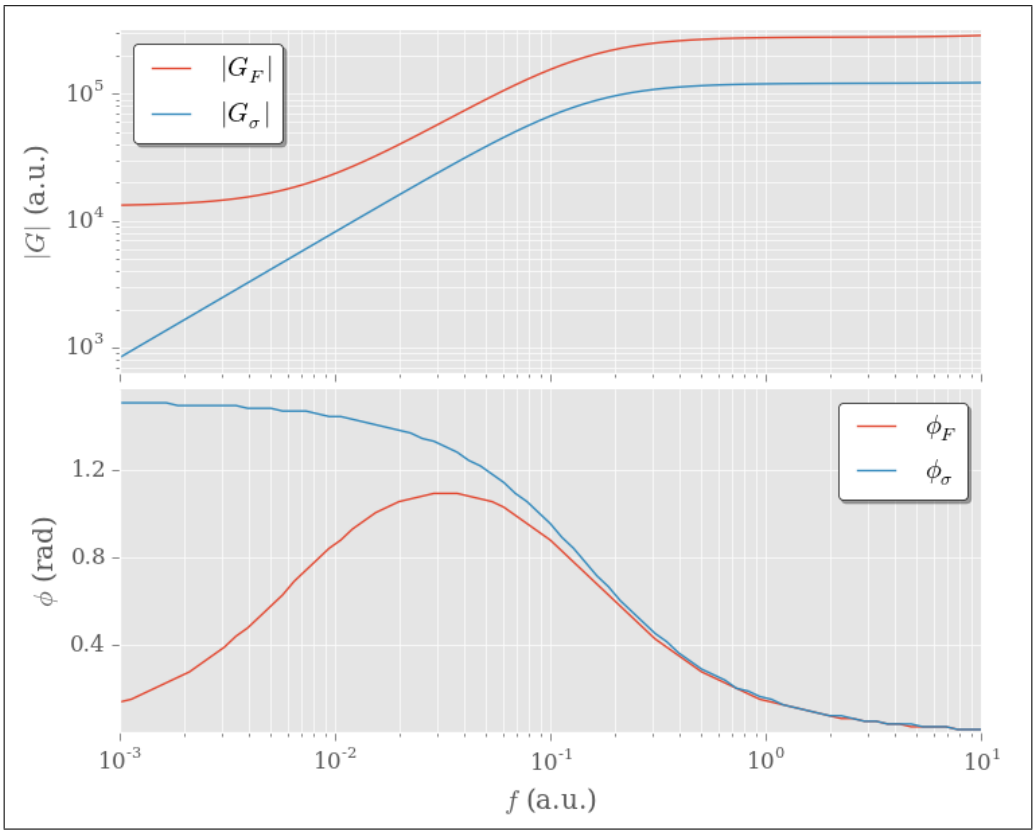

Figure 10: *Steady-state response of F and σ to an harmonic perturbation in a, with $m = 0.01$. f denotes the frequency of the oscillations, $|G|$ and ϕ refer to the modulus and phase of the corresponding transfer functions.*

In the high frequency range, the global mechanical response of the cell G_F clearly appears to be dominated by its rheological behaviour G_σ in figure 10. At lower frequencies, the observed plateau may be understood by noticing that G_σ bears the properties a high-pass filter. Therefore, stress σ strays very little from its stationary value $\sigma_{\text{st}} = m$ in that domain, and the cell behaves as an ordinary drop between two plates with a constant surface tension. Thus, imposed stationary oscillations around its minimal-area configuration give rise to an elastic reaction force on the plates, as the cell attempts to recover its equilibrium shape.
We have here provided a detailed description of a single-cell configuration, along with its treatment within our model. Let us now briefly describe two examples of "crystalline" multicellular arrays, involving multiple identical cells evenly spread on a lattice, which we developed as necessary technical steps towards the study of general aggregates. The equations involved are very similar to the ones presented in this subsection, and will not be detailed again. To our knowledge, these configurations may regrettably not be directly linked to existing experimental setups; we therefore choose not to linger on the obtained results in this report.

2. Chain of identical cells

A natural generalisation of our previous single-cell configuration may be obtained by considering an infinite chain of identical living cells, of which an element is drawn figure 11:

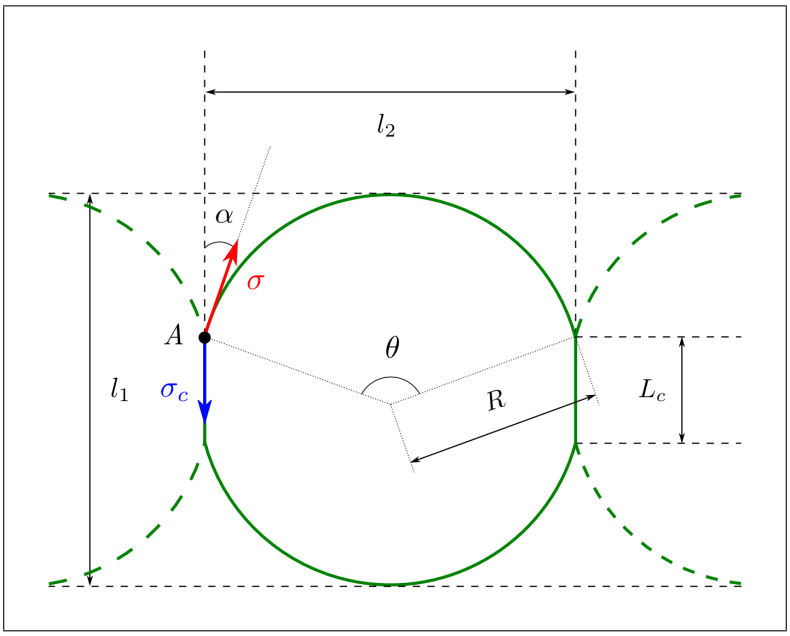

Figure 11: *Living cell as part of an horizontal "1D" aggregate of identical cells.*

For symmetry reasons, the cell-cell contact edges on both sides must remain flat and vertical; we denote their length by L_c. This contact line between two adjacent cell membranes may now develop an additional stress σ_c, and its dynamics may be endowed with a rheological contribution according to (15). Plateau equilibrium relation (2) written at vertex A then reads, projected on the vertical axis:

$$\sigma_c = \sigma \cdot \cos\alpha$$

Note that we *a priori* do not expect the curvature of the free membrane wall to change signs in this

configuration; a simple parametrisation using curvature radius R is thus possible. The axial force F exerted by the cell on its neighbour then reads, on either sides:

$$F = -P \cdot L_c + 2\sigma \cdot \sin\alpha$$

This symmetrical geometry does not take boundary effects into account; therefore, one may numerically evaluate the aggregate bulk mechanical response by externally imposing length l_2, and measuring the reaction force F generated by a single chain link. Reciprocically, the geometrical response of the aggregate to an external force may be assessed by imposing force F and computing the evolutions of the corresponding variables figure 11.

3. Rectangular-lattice tissue

Before undertaking the treatment of general 2D aggregates, one may finally mention the case of identical cells spread on a rectangular lattice. In this fixed geometry, each cell always remains in contact with four immediate neighbours; a "corner" of such a cell is drawn figure 12, the rest of the aggregate being inferred by symmetry:

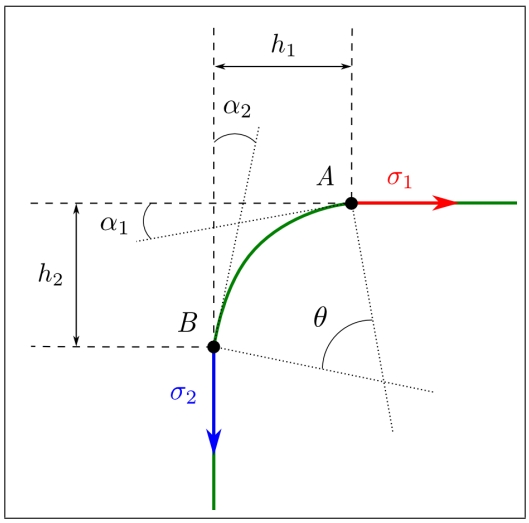

Figure 12: *Corner of a cell within the rectangular lattice geometry.*

The cells now bears two independent flat contact sides, respectively denoted by indices 1 and 2, whose dynamical evolutions are ruled by equation (15). Note that the curved free membrane wall acts here as an interface with a cavity in the bulk of our cell aggregate, similar to the well-known **Plateau borders** observed in wet foams[17].

Generalised equilibrium relation (2) may be written at vertices A and B as follows:

$$\sigma_1 = \sigma \cdot \cos\alpha_1$$
$$\sigma_2 = \sigma \cdot \cos\alpha_2$$

where σ denotes the stress of the free membrane wall. The considerations leading to the remaining equations are then very similar to the cases tackled above; let us thus move on to next section and provide a short discussion on general, non-symmetrical aggregates.

[17] The mathematical link between Plateau borders and Plateau equilibrium as defined in (ii) for dry foams is then given by the so-called **decoration theorem**; a thorough discussion of the subject is given in [5].

IV. General Geometry

We now wish to outline the means by which one may generalise the resolution method developed in the previous sections to ordinary living tissues. We will therefore provide the parametrisation to be used in the case of a generic two-cell contact involving non-identical cells, bearing in mind the remarks elicited in III.1. A breakdown of the equations and variables to be used at the scale of the tissue will finally be imparted, so as to provide a general proof of equality (35).

1. Parametrisation

The general parametrisation describing a system of two cells in contact is depicted figure 13. The full system of equations used to compute their evolution is detailed in appendix B; let us only discuss here the few equations that qualitatively differ from our previous considerations.

The curvature C_c of the two membrane edges in contact is now non-zero, and may be linked to the pressure difference between the two cells through the Laplace law. Let us index by subscripts 0 and 1 the two membranes in contact, and denote by L_c their common curvilinear length. In the general case, stresses σ_0 and σ_1 may differ, but the strains must remain equal within both segments:

$$\dot{\sigma_0} + \sigma_0 - m_l = \dot{\sigma_1} + \sigma_1 - m_r \tag{49}$$

where we have used (10), denoting by m_l and m_r the respective contractilities of the left and right cells. Using the convention that $C_c > 0$ if $h > 0$, the pressure drop between the two cells reads:

$$P_r - P_l = C_c \cdot (\sigma_0 + \sigma_1) \tag{50}$$

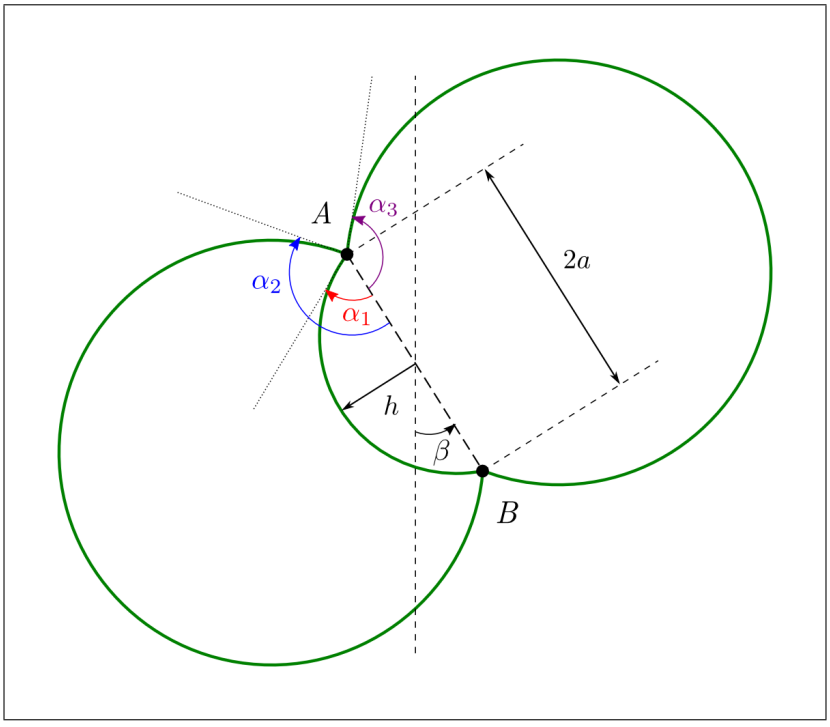

Figure 13: *General contact between two non-identical cells.*

Interestingly, equation (50) may be recovered through a linear combination of Laplace relation (3), written for both free membrane edges, and Plateau equilibrium relation (2) projected on the normal to the chord AB, as demonstrated in appendix B. Intuitively, this equivalency may be understood by recalling that the Laplace equation stems from the balance of normal stresses across an interface at equilibrium (cf. II.1.b); as such, it generally bears some degree of redundancy with Plateau relation (2).
Consequently, equation (50) need not be used by our resolution algorithm, whose convergence relies on the linear independence of the system of equations used. Let us thus proceed to account for the correct equations and variables ensuring a non-redundant description of generic living tissues comprised of an arbitrary number of cells.

2. Degrees of freedom

Let us define the following parameters describing the topology of the tissue:
- C the total number of cells
- V the number of vertices
- N_1 the number of edges separating two cells
- N_2 the number of boundary edges with the exterior environment

Denoting by N the number of cavities within the aggregate, one obtains the so-called Euler relation in dimension 2 (see [5]):

$$C + V + N - N_1 - N_2 = 2$$

Bearing in mind the parametrisation previously defined, the variables fully describing the aggregate are the following:
- for each cell: pressure P ..... C **unknowns**
- for each vertex: two coordinates (x, y) ..... $2V$ **unknowns**
- for each edge: curvilinear length L, chord length a, angle α w.r.t. the chord, height h, curvature C and chord orientation β ..... $6(N_1 + N_2)$ **unknowns**
- for each edge between two cells: two stresses σ_0, σ_1 ..... $2N_1$ **unknowns**
- for each boundary edge: stress σ ..... N_2 **unknowns**

The total number n of variables thus reads:

$$n = C + 2V + 8N_1 + 7N_2 \tag{51}$$

The corresponding equations are listed below:
- for each bubble: a fixed volume condition ..... C **equations**
- for each vertex: a vectorial Plateau equilibrium relation ..... $2V$ **equations**
- for each edge: five geometrical equations, listed in appendix B ..... $5(N_1 + N_2)$ **equations**
- for each edge between two cells: a Laplace relation, a rheological equation and an equal strain condition for the edges in contact ..... $3N_1$ **equations**
- for each boundary edge: a Laplace relation and a rheological equation ..... $2N_2$ **equations**

Using the notations of II.3, we thus recover the equality between n and the total number m of equations:

$$\boxed{m = C + 2V + 8N_1 + 7N_2 = n} \tag{52}$$

Note that following the remarks elicited in IV.1, it may be proven that three equations among all Laplace and Plateau equilibrium relations are redundant at the scale of the aggregate, and must consequently be weeded out. The three resulting degrees of freedom may finally be set by imposing the in-plane position of the tissue centre of mass, along with the bulk orientation of the aggregate.

V. CONCLUSION

Our simplified model has thus far allowed us to accurately reproduce the qualitative mechanical properties of single cells. Its dynamics may easily be interpreted in terms of simple physical arguments, and are very consistent with the experimental observations reported by [1]. Further investigation would be required to assess the quality of our phenomenological cortex rheology, e.g. using the harmonic analysis of single-cell mechanical responses provided by A. Asnacios *et al.*. A generalisation to other potential simple geometries experimentally available would also be desirable, so as to evaluate the limits of our cell-cell adhesion model in different configurations; the details of this model will likely be the subject of an article to be written in the months to come.

The main priority however lies with the extension of our simulations to non-symmetrical tissues, following the considerations detailed in section IV, which may more realistically describe experimentally-obtainable aggregates. So far, only the treatment of generic two-cell contacts as presented in IV.1 could be implemented, due to time constraints; this generalisation would allow us to assess the behaviour of our model within a much wider range of available literature.

Once implemented, this version would further enable us to simulate a broad variety of biological phenomena, including for instance tissue growth dynamics under imposed stress by providing a set of cell division rules, or anisotropic cell contractility by phenomenologically accounting for actin filaments aligning within the cell cortex. In the longer run, it will also provide the framework for a generalisation to 3D aggregates to allow for simplified, yet fully realistic simulations!

REFERENCES

[1] Research page of A. Asnacios, Prof. Paris 7.

[2] Boulbitch, A. (1997). Deflection of a Cell Membrane Under Application of a Local Force, *Physical Review E*, Vol. 57, **2**:2123–2128.

[3] Brackenbury, R., Rutishauser, U. and Edelman, GM. (1981). Distinct Calcium-independent and Calcium-dependent Adhesion Systems of Chicken Embryo Cells, *Proceedings of the National Academy of Science*, **78**(1):387–391.

[4] Campàs, O., Mammoto, T., Hasso, S. *et al.* (2013). Quantifying Cell-Generated Mechanical Forces Within Living Embryonic Tissues, *Nature Methods*, **11**:183–189.

[5] Cantat, I., Cohen-Addad, S., Elias, F., Graner, F., Höhler, R., Pitois, O., Rouyer, F. and Saint-Jalmes, A. (2010). *Foams: Structure and Dynamics*, pp. 59–61, Oxford University Press.

[6] Étienne, J., Asnacios, A., Mitrossilis, D., Peschetola, V. and Verdier, C. (2011). How the Cell Got its Shape: a Visco-Elasto-Active Model of the Cytoskeleton, *20e Congrès Français de Mécanique*.

[7] Glazier, J. and Graner, F. (1993). Simulation of the Differential Adhesion-Driven Rearrangement of Biological Cells, *Physical Review E*, Vol. 47, **3**:2129–2154.

[8] Gonzalez-Rodriguez, D., Guevorkian, K., Douezan, S. and Brochard-Wyart, F. (2012). Soft-Matter Models of Developing Tissues and Tumors, *Science*, **338**:910–917.

[9] Heisenberg, CP. and Bellaïche, Y. (2013). Forces in Tissue Morphogenesis and Patterning, *Cell*, Vol. 153, **5**:948–962.

[10] Ipsen, I. (2009). *Numerical Matrix Analysis*, pp. 44–51.

[11] Keller, R. (2012). Physical Biology Returns to Morphogenesis, *Science*, **338**:201–203.

[12] Li, D., Zhou, J., Chowdhury, F. *et al.* (2011). Role of Mechanical Factors in Fate Decisions of Stem Cells, *Regenerative Medicine*, **6**(2):229–240.

[13] Magner, L. (2002). *A History of the Life Sciences: Third Edition, Revised and Expanded*, pp. 195–201, CRC Press.

[14] Martz, E., Phillips, H. and Steinberg, M. (1974). Contact Inhibition of Overlapping and Differential Cell Adhesion: A Sufficient Model for the Control of Certain Cell Culture Morphologies, *Journal of Cell Science*, **16**:401–419.

[15] Nelson, W. (2008). Regulation of Cell-cell Adhesion by the Cadherin-catenin Complex, *Biochemical Society Transactions*, **36**(2):149–155.

[16] Ponti, A., Machacek, M. *et al.* (2004). Two Distinct Actin Networks Drive the Protrusion of Migrating Cells, *Science*, **305**:1782–1786.

[17] Reddi, AH. (2000). Morphogenesis and Tissue Engineering of Bone and Cartilage: Inductive Signals, Stem Cells, and Biomimetic Biomaterials, *Tissue Engineering*, **6**(4):351–359.

[18] Roux, W. (1888). Beitrage zur Entwicklungsmechnik des Embryo, *Virchows Arch. Pathol. Anat. Physiol. Klin. Med.*, **114**:113–153.

[19] Taylor, J. (1976). The Structure of Singularities in Soap-bubble-like and Soap-film-like Minimal Surfaces, *Annals of Mathematics. Second Series*, **103**(3):489–539.

A. COMPLEMENTS ON GEOMETRY

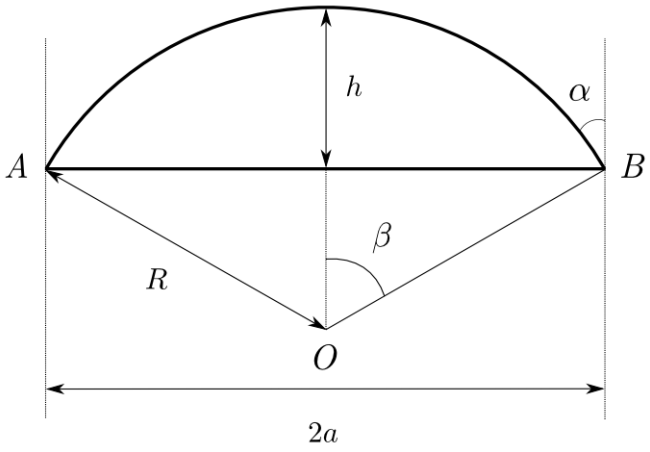

Figure 14: *Circular segment, chord and height.*

We wish to compute the area S of the circular segment, delimited by the bold contour figure 14, as a function of α, a and h. It may be defined as the area of the total circle arc AB, minus the area of triangle AOB:

$$S = R^2 \cdot \beta - R^2 \cdot \sin\beta \cos\beta \tag{53}$$

Furthermore, one easily obtains the following relations:

$$\alpha = \frac{\pi}{2} - \beta \tag{54}$$

$$a = R \cdot \sin\beta = R \cdot \cos\alpha \tag{55}$$

$$h = R \cdot (1 - \cos\beta) = R \cdot (1 - \sin\alpha) \tag{56}$$

The curvilinear length L of circle arc AB is then given by:

$$\boxed{L = 2R \cdot \beta = R \cdot (\pi - 2\alpha)} \tag{57}$$

Dividing (56) by (55):

$$\frac{h}{a} = \frac{1 - \cos\beta}{\sin\beta} = \frac{2 \cdot \left(1 - \cos^2\frac{\beta}{2}\right)}{2 \cdot \cos\frac{\beta}{2} \sin\frac{\beta}{2}}$$

$$\boxed{\frac{h}{a} = \tan\frac{\beta}{2} = \tan\left(\frac{\pi}{4} - \frac{\alpha}{2}\right)} \tag{58}$$

Consequently, using (55) and (58):

$$\begin{aligned} S &= R^2 \cdot (\beta - \sin\beta\cos\beta) \\ &= \frac{a^2}{\sin^2\beta} \cdot (\beta - \sin\beta\cos\beta) \\ &= \frac{ah}{\tan\frac{\beta}{2}\sin^2\beta} \cdot (\beta - \sin\beta\cos\beta) \\ &= ah \cdot \frac{\beta - \sin\beta\cos\beta}{4\sin^3\frac{\beta}{2}\cos\frac{\beta}{2}} \\ &= ah \cdot \frac{\beta - \sin\beta\cos\beta}{4\tan^3\frac{\beta}{2}\cos^4\frac{\beta}{2}} \end{aligned}$$

S may thus be written in the form:

$$S = ah \cdot \frac{\left(1+\tan^2\frac{\beta}{2}\right) \cdot \left[\left(1+\tan^2\frac{\beta}{2}\right)\beta - 2\tan\frac{\beta}{2}\cos\beta\right]}{4\tan^3\frac{\beta}{2}} \tag{59}$$

where we have used trigonometric identity:

$$\frac{1}{\cos^2\frac{\beta}{2}} = 1 + \tan^2\frac{\beta}{2}$$

One may notice that

$$\begin{aligned} \left(1+\tan^2\frac{\beta}{2}\right) \cdot \cos\beta &= \left(1+\tan^2\frac{\beta}{2}\right) \cdot \left(2\cos^2\frac{\beta}{2} - 1\right) \\ &= 2 - \left(1+\tan^2\frac{\beta}{2}\right) \end{aligned}$$

which allows us to rewrite (59) as follows:

$$S = ah \cdot \frac{\left(1+\tan^2\frac{\beta}{2}\right)^2 \cdot \beta - 4\tan\frac{\beta}{2} + 2\tan\frac{\beta}{2}\left(1+\tan^2\frac{\beta}{2}\right)}{4\tan^3\frac{\beta}{2}} \tag{60}$$

Let us define

$$f_V(\beta) = \frac{\left(1+\tan^2\frac{\beta}{2}\right)^2 \cdot \beta - 2\tan\frac{\beta}{2} + 2\tan^3\frac{\beta}{2}}{4\tan^3\frac{\beta}{2}} \tag{61}$$

(54), (60) and (61) finally yield:

$$\boxed{S = ah \cdot f_V(\frac{\pi}{2} - \alpha)} \tag{62}$$

One may further prove that f_V is continuous and differentiable as β goes to 0, and that:

$$\begin{aligned} f_V(0) &= \frac{4}{3} \\ \frac{df_V}{d\beta}(0) &= 0 \end{aligned}$$

B. General resolution of a cell-cell contact

Let us enumerate below the equations and variables determining the dynamics of two generic cells in contact within our model, using the notations of figure 13.

- Cell incompressibility:

$$V_l = f_V(\alpha_1) \cdot ah - R_2^2 \cdot \left[\alpha_2 - \frac{\sin(2\alpha_2)}{2}\right] \tag{63}$$

$$V_r = -f_V(\alpha_1) \cdot ah + R_3^2 \cdot \left[\alpha_3 - \frac{\sin(2\alpha_3)}{2}\right] \tag{64}$$

  where V_l and V_r refer to the respective volumes of the left and right cells, and f_V to the area of the circular contact segment per unit height and chord defined in (61).

- Chord lengths from arc lengths and angles, counting angles positively counterclockwise:

$$L_c \cdot \operatorname{sinc} \alpha_1 = 2a \tag{65}$$

$$L_2 \cdot \operatorname{sinc} \alpha_2 = 2a \tag{66}$$

$$L_3 \cdot \operatorname{sinc} \alpha_3 = 2a \tag{67}$$

- Other geometrical constraints directly inferred from appendix A, using the sign conventions of IV.1:

$$h \cdot \cos\frac{\alpha_1}{2} = a \cdot \sin\frac{\alpha_1}{2} \tag{68}$$

$$2\alpha_1 = -L_c \cdot C_c \tag{69}$$

$$L_2 = -2R_2 \cdot \alpha_2 \tag{70}$$

$$L_3 = 2R_3 \cdot \alpha_3 \tag{71}$$

- Vertex coordinates from chord length and inclination angle, projected on x and y:

$$x_B - x_A = -2a \cdot \sin\beta \tag{72}$$

$$y_B - y_A = 2a \cdot \cos\beta \tag{73}$$

- Vertex "center of mass" fixed at the origin, projected on x and y:

$$x_A + x_B = 0 \tag{74}$$

$$y_A + y_B = 0 \tag{75}$$

- Vectorial Plateau relation (2), written at either vertex A or B, projected on the chord and its normal:

$$(\sigma_0 + \sigma_1) \cdot \cos\alpha_1 + \sigma_2 \cdot \cos\alpha_2 + \sigma_3 \cdot \cos\alpha_3 = 0 \tag{76}$$

$$(\sigma_0 + \sigma_1) \cdot \sin\alpha_1 + \sigma_2 \cdot \sin\alpha_2 + \sigma_3 \cdot \sin\alpha_3 = 0 \tag{77}$$

- Equal strains for both sides of a contact zone:

$$\dot{\sigma_0} + \sigma_0 - m_l = \dot{\sigma_1} + \sigma_1 - m_r \tag{78}$$

  where subscripts l and r respectively denote the left and right cell.

- Dynamical rheology relations for each independent side:

$$\dot{L_c} = L_c \cdot (\dot{\sigma_0} + \sigma_0 - m_l) + 2v_{\text{ca}} \tag{79}$$
$$\dot{L_2} = L_2 \cdot (\dot{\sigma_2} + \sigma_2 - m_l) - 2v_{\text{ca}} \tag{80}$$
$$\dot{L_3} = L_3 \cdot (\dot{\sigma_3} + \sigma_3 - m_r) - 2v_{\text{ca}} \tag{81}$$

- Laplace overpressures at each free interface:

$$P_l = \frac{\sigma_2}{R_2} \tag{82}$$
$$P_r = \frac{\sigma_3}{R_3} \tag{83}$$

Hence, the 5 geometrical equations fully describing a membrane edge as a circle arc within our model may be summarised as follows, using the generic notations introduced figures 13 and 14:

$$\begin{aligned} L \cdot \operatorname{sinc} \alpha &= 2a \\ h \cdot \cos \frac{\alpha}{2} &= a \cdot \sin \frac{\alpha}{2} \\ L \cdot C &= 2\alpha \\ x_B - x_A &= -2a \cdot \sin \beta \\ y_B - y_A &= 2a \cdot \cos \beta \end{aligned}$$

Assuming bulk-rotation angle β to be fixed, we obtain a system of 21 independent equations (63)–(83) involving 21 different variables. However, we have here omitted to write Laplace relation (50) across the interface between the two cells, which should yield an additional equation for the same number of variables. Let us thus prove that this relation is redundant with our set of equations, to ensure the system is not over-determined.

Using (82) and (83), one may write:

$$P_r - P_l = \frac{\sigma_3}{R_3} - \frac{\sigma_2}{R_2}$$

Substituting (70) and (71) for R_2 and R_3:

$$\begin{aligned} P_r - P_l &= \frac{2\alpha_3 \cdot \sigma_3}{L_3} + \frac{2\alpha_2 \cdot \sigma_2}{L_2} \\ &= \frac{\sigma_3 \cdot \sin \alpha_3 + \sigma_4 \cdot \sin \alpha_4}{a} \end{aligned}$$

where we have used (66) and (67). Equation (77) further yields:

$$P_r - P_l = -\frac{(\sigma_0 + \sigma_1) \cdot \sin \alpha_1}{a}$$

Finally, substituting (65) for a and using (69), one recovers the expected relation:

$$\boxed{P_r - P_l = -\frac{2\alpha_1 \cdot (\sigma_0 + \sigma_1)}{L_c} = C_c \cdot (\sigma_0 + \sigma_1)}$$

C. CADHERIN CURVATURE DERIVATION

Using the notations of II.2.c, we assume the microscopic curvature C_μ, membrane bending modulus κ and macroscopic stress σ to be such that:

$$C_\mu \ll \sqrt{\frac{\sigma}{\kappa}}$$

so as to neglect forces arising from local membrane bending. The microscopic stress σ_μ conveyed by an infinitesimal membrane element ds in the adhesion zone is thus purely tangential, and one can write:

$$\sigma_x(s) = \sigma_\mu(s) \cdot \cos\theta(s) \tag{84}$$
$$\sigma_y(s) = \sigma_\mu(s) \cdot \sin\theta(s) \tag{85}$$

where σ_x and σ_y denote the stress components borne by the contact line and its normal, respectively. The projected mechanical equilibrium then reads:

$$\frac{d\sigma_x}{ds} = -P \cdot \sin\theta \tag{86}$$
$$\frac{d\sigma_y}{ds} = P \cdot \cos\theta + c \cdot F_0 \tag{87}$$

with c the average cadherin concentration within the contact zone, F_0 the average force exerted by a single cadherin and P the overpressure within the cell. (84) and (85) yield:

$$\sigma_y(s) = \sigma_x(s) \cdot \tan\theta(s) \tag{88}$$

Differentiating (88) with respect to s:

$$\frac{d\sigma_y}{ds} = (1+\tan^2\theta) \cdot \frac{d\theta}{ds} \cdot \sigma_x + \tan\theta \cdot \frac{d\sigma_x}{ds}$$

Replacing σ derivatives by their expressions from (86) and (87):

$$P\cos\theta + cF_0 = (1+\tan^2\theta)\theta'\sigma_x + \tan\theta\,[-P\sin\theta]$$
$$P + cF_0\cos\theta = (1+\tan^2\theta)\theta'\sigma_x\cos\theta = \theta'\frac{\sigma_x}{\cos\theta}$$

Using (84), one gets a first relation linking the local curvature $C_\mu(\theta)$ to the mechanical parameters:

$$\boxed{C_\mu(\theta) = \theta'(s) = \frac{P + cF_0\cos\theta}{\sigma_\mu(\theta)}} \tag{89}$$

We can rewrite (89) in the form:

$$\sigma_x(s) = \frac{P\cos\theta(s) + cF_0\cos^2\theta(s)}{\theta'(s)} \tag{90}$$

Differentiating (90) with respect to s, and using (86) again, one obtains:

$$\frac{d\sigma_x}{ds} = \frac{(-P\sin\theta - 2cF_0\sin\theta\cos\theta)\,\theta'}{\theta'} - \frac{\theta''}{\theta'^2}\left(P\cos\theta + cF_0\cos^2\theta\right)$$
$$-P\sin\theta = -P\sin\theta - 2cF_0\sin\theta\cos\theta - \frac{\theta''}{\theta'^2}\left(P\cos\theta + cF_0\cos^2\theta\right)$$

which finally yields:

$$\frac{\theta''}{\theta'} = -\frac{2cF_0 \sin\theta}{P + cF_0 \cos\theta} \cdot \theta' \tag{91}$$

Let us define ψ as follows:

$$\psi = \frac{cF_0}{P} \tag{92}$$

We integrate (91) with respect to s:

$$\log(\theta') = 2\log\left(1 + \psi\cos\theta\right) + \text{cst.}$$

$$\boxed{\theta'(s) = C_\mu(\theta) = K \cdot \left[1 + \psi\cos\theta\right]^2} \tag{93}$$

Comparing (93) and (89) yields the following expression for σ_μ:

$$\sigma_\mu(\theta) = \frac{P}{K \cdot (1 + \psi\cos\theta)} \tag{94}$$

To determine K, we define as α_h the angle such that $h(\alpha_h) = h_{\text{ca}}$. One must therefore leave the microscopic contact zone and recover the macroscopic membrane properties as soon as $\theta \geq \alpha_h$. The membrane stress continuity written in $\theta = \alpha_h$ thus imposes:

$$\sigma_\mu(\theta = \alpha_h) = \sigma$$

with σ the macroscopic membrane stress. Using (94), the corresponding expression for K reads:

$$\boxed{K = \frac{C}{1 + \psi\cos\alpha_h}} \tag{95}$$

with C the macroscopic curvature given by the Laplace law:

$$C = \frac{P}{\sigma} \tag{96}$$

Thus, (93) and (94) become:

$$C_\mu(\theta) = C \cdot \frac{\left(1 + \psi\cos\theta\right)^2}{1 + \psi\cos\alpha_h} \tag{97}$$

$$\sigma_\mu(\theta) = \sigma \cdot \frac{1 + \psi\cos\alpha_h}{1 + \psi\cos\theta} \tag{98}$$

From (97), one notices that ψ quantifies the curvature break from the macroscopic curvature C in $\theta = \alpha_h$, due to the local cadherin forces.

Similarly in $\theta = 0$, one reaches the macroscopic contact zone, and one must recover the macroscopic stress given by the Plateau relation:

$$\sigma_\mu(\theta = 0) = \sigma_c = \sigma \cdot \cos\alpha \tag{99}$$

with σ_c the stress of the membranes in contact. Substituting (98) in (99) yields an additional relation between α_h, ψ and the macroscopic angle α:

$$1 + \psi \cdot \cos\alpha_h = (1 + \psi) \cdot \cos\alpha \tag{100}$$

Furthermore, h_{ca} and α_h are linked to the microscopic curvature through the integral relation:

$$h_{\mathrm{ca}} = \int_0^h dy = \int_0^{\delta s} ds \sin\theta(s) = \int_0^{\alpha_h} \frac{d\theta}{C_\mu(\theta)} \sin\theta$$

Substituting (93) for $C_\mu(\theta)$,

$$\begin{aligned} h_{\mathrm{ca}} &= \frac{1}{K} \cdot \int_0^{\alpha_h} d\theta \frac{\sin\theta}{(1+\psi\cos\theta)^2} \\ &= \frac{1}{K} \cdot \int_{\cos\alpha_h}^1 \frac{du}{(1+\psi u)^2} \\ &= \frac{1}{K\psi} \cdot \left[-\frac{1}{1+\psi u} \right]_{\cos\alpha_h}^1 \\ &= \frac{1}{K\psi(1+\psi)} \cdot \left(\frac{1}{\cos\alpha} - 1 \right) \end{aligned}$$

where we have used relation (100). Substituting for K,

$$h_{\mathrm{ca}} = \frac{1+\psi\cos\alpha_h}{\psi C(1+\psi)} \cdot \left(\frac{1}{\cos\alpha} - 1 \right) = \frac{1}{\psi C} \cdot (1-\cos\alpha)$$

Substituting (92) for ψ and using (96), we obtain one last relation:

$$\boxed{c = \frac{\sigma}{h_{\mathrm{ca}} F_0} \cdot (1-\cos\alpha)} \tag{101}$$

which determines the value of c from microscopic constants h_{ca}, F_0 and macroscopic variables σ, α. Thus,

$$\psi = \frac{cF_0}{P} = \frac{1}{h_{\mathrm{ca}} C} \cdot (1-\cos\alpha) \tag{102}$$

where we have substituted (96) for P. One may then rewrite (100) in the form:

$$\cos\alpha_h = \cos\alpha + \frac{\cos\alpha - 1}{\psi} \tag{103}$$

Plugging (102) into (103) finally yields:

$$\boxed{\cos\alpha_h = \cos\alpha - \frac{h_{\mathrm{ca}}}{R}} \tag{104}$$

with $R = 1/C$ the macroscopic curvature radius. Note that (104) may also be recovered from figure 7b, using some basic geometry. Assuming cadherin interactions to be short-range, $h_{\mathrm{ca}}/R \ll 1$ and (104) imposes

$$\alpha_h \simeq \alpha$$

D. CADHERIN CURVATURE INTEGRAL

We now wish to compute the total membrane length δs of the microscopic adhering area, given by the integral:

$$\delta s = \int_0^{\alpha_h} \frac{d\theta}{C_\mu(\theta)} = \frac{1}{K} \cdot \int_0^{\alpha_h} \frac{d\theta}{(1+\psi\cos\theta)^2} \tag{105}$$

Regrettably, (105) does not display any of the canonical Bioche symmetries as an integral of a rational trigonometric function. One has to resort to the change of variable $t = \tan\frac{\theta}{2}$, with the identities:

$$d\theta = \frac{2dt}{1+t^2}$$
$$\cos\theta = \frac{1-t^2}{1+t^2}$$

(105) becomes:

$$\delta s = \frac{2}{K} \cdot \int_0^{\tan\frac{\alpha_h}{2}} f(t)dt \tag{106}$$

with

$$\boxed{f(t) = \frac{(1+t^2)}{\left[(1-\psi)t^2+\psi+1\right]^2}} \tag{107}$$

- If $\psi < 1$:

$$\begin{aligned} f(t) = & \quad \frac{1}{1-\psi} \cdot \frac{1}{(1-\psi)t^2+\psi+1} - \frac{2\psi}{1-\psi} \cdot \frac{1}{\left[(1-\psi)t^2+\psi+1\right]^2} \\ \equiv & \quad g(t) - h(t) \end{aligned}$$

because

$$1+t^2 = \left[(1-\psi)t^2+\psi+1\right] \cdot \frac{1}{1-\psi} - \frac{1+\psi}{1-\psi} + 1$$

  - Integral of g:

$$\begin{aligned} \int_0^{\tan\frac{\alpha_h}{2}} g(t)dt &= \frac{1}{(1-\psi)^2} \cdot \int_0^{\tan\frac{\alpha_h}{2}} \frac{dt}{t^2+\frac{1+\psi}{1-\psi}} \\ &= \frac{1}{(1-\psi)^2} \cdot \left[\sqrt{\frac{1-\psi}{1+\psi}}\arctan\left(t\sqrt{\frac{1-\psi}{1+\psi}}\right)\right]_0^{\tan\frac{\alpha_h}{2}} \end{aligned}$$

Let us define

$$\phi = \frac{1-\psi}{1+\psi} \tag{108}$$
$$\beta = \sqrt{\phi}\tan\frac{\alpha_h}{2} \tag{109}$$

The integral yields:

$$\boxed{\int_0^{\tan\frac{\alpha_h}{2}} g(t)dt = \frac{1}{(1-\psi)\sqrt{1-\psi^2}} \cdot \arctan\beta} \tag{110}$$

– Integral of h: Let us use a first change of variable:

$$t' = t\sqrt{\phi}$$

The integral becomes:

$$\begin{aligned}\int_0^{\tan\frac{\alpha_h}{2}} h(t)dt &= \frac{2\psi}{(1-\psi)^3}\cdot\int_0^{\tan\frac{\alpha_h}{2}} \frac{dt}{\left(t^2+\frac{1+\psi}{1-\psi}\right)^2} \\ &= \frac{2\psi\phi^2}{(1-\psi)^3}\cdot\int_0^{\sqrt{\phi}\tan\frac{\alpha_h}{2}} \frac{dt'}{\sqrt{\phi}}\frac{1}{(t'^2+1)^2} \\ &= 2\psi\left(\frac{\sqrt{\phi}}{1-\psi}\right)^3\cdot\int_0^{\beta}\frac{dt'}{(1+t'^2)^2}\end{aligned}$$

Let us further define the following change of variable:

$$\begin{aligned}t' &= \tan y \\ dt' &= \frac{dy}{\cos^2 y}\end{aligned}$$

$$\begin{aligned}\int_0^{\tan\frac{\alpha_h}{2}} h(t)dt &= \frac{2\psi}{(1-\psi^2)^{3/2}}\cdot\int_0^{\arctan\beta}\frac{dy}{\cos^2 y}\frac{1}{(1+\tan^2 y)^2} \\ &= \frac{2\psi}{(1-\psi^2)^{3/2}}\cdot\int_0^{\arctan\beta} dy\cos^2 y \\ &= \frac{\psi}{(1-\psi^2)^{3/2}}\cdot\int_0^{\arctan\beta} dy[1+\cos(2y)]\end{aligned}$$

$$\boxed{\int_0^{\tan\frac{\alpha_h}{2}} h(t)dt = \frac{1}{(1-\psi)\sqrt{1-\psi^2}}\frac{\psi}{1+\psi}\cdot\left[\arctan\beta+\frac{1}{2}\sin(2\arctan\beta)\right]} \tag{111}$$

Then, (110) and (111) yield:

$$\begin{aligned}\delta s &= \frac{2}{K}\cdot\int_0^{\tan\frac{\alpha_h}{2}}[g(t)-h(t)]dt \\ &= \frac{2}{K}\cdot\frac{1}{(1-\psi)\sqrt{1-\psi^2}}\left(\arctan\beta-\frac{\psi}{1+\psi}\left[\arctan\beta+\frac{1}{2}\sin(2\arctan\beta)\right]\right)\end{aligned}$$

$$\boxed{\delta s = \frac{1}{K(1-\psi^2)^{3/2}}\cdot[2\arctan\beta-\psi\sin(2\arctan\beta)]} \tag{112}$$

- If $\psi > 1$: f bears two real poles of order 2: $\pm t_0$, with $t_0 = \sqrt{\frac{\psi+1}{\psi-1}}$. The partial fraction expansion of f reads:

$$f(t) = \frac{a}{t+t_0}+\frac{b}{(t+t_0)^2}+\frac{c}{t-t_0}+\frac{d}{(t-t_0)^2} \tag{113}$$

The parity $f(t) = f(-t)$ imposes the following relations on the coefficients:

$$c = -a \tag{114}$$

$$d = b \tag{115}$$

Multiplying (113) by $(t+t_0)^2$ and evaluating in $t = -t_0$ yields:

$$\begin{aligned} b &= \frac{1+t_0^2}{(\psi-1)^2 \cdot (-2t_0)^2} \\ &= \frac{1+\frac{\psi+1}{\psi-1}}{4(\psi-1)^2 \cdot \frac{\psi+1}{\psi-1}} \\ &= \frac{\psi}{2(\psi-1)(\psi^2-1)} \end{aligned}$$

Then,

$$\begin{aligned} f(t) - \frac{b}{(t+t_0)^2} &= \frac{1+t^2-b(\psi-1)^2 \cdot (t-t_0)^2}{(\psi-1)^2(t-t_0)^2(t+t_0)^2} \\ &= \frac{1+t^2-\frac{1+t_0^2}{4t_0^2} \cdot (t-t_0)^2}{(\psi-1)^2(t-t_0)^2(t+t_0)^2} \\ &= \frac{t^2 \cdot \frac{3t_0^2-1}{4t_0^2} + 2t \cdot \frac{1+t_0^2}{4t_0} + \frac{3-t_0^2}{4}}{(\psi-1)^2(t-t_0)^2(t+t_0)^2} \\ &= \frac{\left(t \cdot \frac{3t_0^2-1}{4t_0^2} + \frac{3-t_0^2}{4t_0}\right) \cdot (t+t_0)}{(\psi-1)^2(t-t_0)^2(t+t_0)^2} \end{aligned}$$

Thus :

$$f(t) - \frac{b}{(t+t_0)^2} = \frac{t \cdot \frac{3t_0^2-1}{4t_0^2} + \frac{3-t_0^2}{4t_0}}{(\psi-1)^2(t-t_0)^2 \cdot (t+t_0)} \tag{116}$$

Multiplying (116) by $t+t_0$ and evaluating again in $t = -t_0$:

$$\begin{aligned} a &= \frac{\frac{1-3t_0^2}{4t_0} + \frac{3-t_0^2}{4t_0}}{(\psi-1)^2 \cdot (-2t_0)^2} \\ &= \frac{1}{16t_0^3} \cdot \frac{4-4t_0^2}{(\psi-1)^2} \\ &= \frac{1}{4} \frac{1-\frac{\psi+1}{\psi-1}}{(\psi-1)^2 \cdot \frac{\psi+1}{\psi-1}\sqrt{\frac{\psi+1}{\psi-1}}} \\ &= -\frac{1}{2} \frac{1}{(\psi-1)^2 \cdot (\psi+1)\sqrt{\frac{\psi+1}{\psi-1}}} \\ &= -\frac{1}{2(\psi^2-1)^{3/2}} \end{aligned}$$

Substituting the computed coefficients in (113):

$$\boxed{f(t) = \frac{\psi}{2(\psi-1)(\psi^2-1)} \cdot \left[\frac{1}{(t+t_0)^2} + \frac{1}{(t-t_0)^2}\right] + \frac{1}{2(\psi^2-1)^{3/2}} \cdot \left[\frac{1}{t-t_0} - \frac{1}{t+t_0}\right]} \tag{117}$$

One must have $\alpha_h \leq \frac{\pi}{2}$ for cadherins to be able to physically interact with one another. Therefore,

$$\begin{cases} t_0 = \sqrt{\dfrac{\psi+1}{\psi-1}} > 1 \\ \tan\dfrac{\alpha_h}{2} \leq 1 \end{cases}$$

Hence $\left[0, \tan\frac{\alpha_h}{2}\right]$ does not hold any poles of f, and f is fully integrable on this interval. Let us define g,h such that

$$g(t) = \frac{\psi}{2(\psi-1)(\psi^2-1)} \cdot \left[\frac{1}{(t+t_0)^2} + \frac{1}{(t-t_0)^2}\right] \tag{118}$$

$$h(t) = \frac{1}{2(\psi^2-1)^{3/2}} \cdot \left[\frac{1}{t-t_0} - \frac{1}{t+t_0}\right] \tag{119}$$

One can then simply rewrite (117) as:

$$f(t) = g(t) + h(t)$$

– Integral of g:

$$\begin{aligned}
\int_0^{\tan\frac{\alpha_h}{2}} g(t)dt &= -\frac{\psi}{2(\psi-1)(\psi^2-1)} \cdot \left[\frac{1}{t+t_0} + \frac{1}{t-t_0}\right]_0^{\tan\frac{\alpha_h}{2}} \\
&= -\frac{\psi}{2(\psi-1)(\psi^2-1)} \cdot \left[\frac{1}{\tan\frac{\alpha_h}{2}+t_0} + \frac{1}{\tan\frac{\alpha_h}{2}-t_0}\right] \\
&= \frac{\psi}{2(\psi-1)(\psi^2-1)} \cdot \frac{2\tan\frac{\alpha_h}{2}}{t_0^2 - \tan^2\frac{\alpha_h}{2}} \\
&= \frac{\psi}{(\psi-1)(\psi^2-1)} \cdot \frac{\tan\frac{\alpha_h}{2}}{\frac{\psi+1}{\psi-1} - \tan^2\frac{\alpha_h}{2}} \\
&= \frac{\psi}{(\psi+1)^2(\psi-1)} \cdot \sqrt{\frac{\psi+1}{\psi-1}} \cdot \frac{\sqrt{\frac{\psi-1}{\psi+1}}\tan\frac{\alpha_h}{2}}{1 - \frac{\psi-1}{\psi+1}\tan^2\frac{\alpha_h}{2}}
\end{aligned}$$

Let us now define

$$\phi = \frac{\psi-1}{\psi+1} \tag{120}$$

$$\beta = \sqrt{\phi}\tan\frac{\alpha_h}{2} \tag{121}$$

We obtain :

$$\boxed{\int_0^{\tan\frac{\alpha_h}{2}} g(t)dt = \frac{\psi}{(\psi^2-1)^{3/2}} \cdot \frac{\beta}{1-\beta^2}} \tag{122}$$

– Integral of h:

$$\begin{aligned}
\int_0^{\tan\frac{\alpha_h}{2}} h(t)dt &= \frac{1}{2(\psi^2-1)^{3/2}} \cdot \left[\log(t_0-t) - \log(t_0+t)\right]_0^{\tan\frac{\alpha_h}{2}} \\
&= -\frac{1}{2(\psi^2-1)^{3/2}} \cdot \log\left(\frac{t_0+\tan\frac{\alpha_h}{2}}{t_0-\tan\frac{\alpha_h}{2}}\right) \\
&= -\frac{1}{2(\psi^2-1)^{3/2}} \cdot \log\left(\frac{1+\beta}{1-\beta}\right)
\end{aligned}$$

Recognising the logarithmic representation of the inverse hyperbolic tangent:

$$\boxed{\int_0^{\tan\frac{\alpha_h}{2}} h(t)dt = -\frac{1}{(\psi^2-1)^{3/2}}\cdot \text{artanh}\beta} \tag{123}$$

(122) and (123) then yield:

$$\begin{aligned}\delta s &= \frac{2}{K}\cdot\int_0^{\tan\frac{\alpha_h}{2}}[g(t)+h(t)]dt \\ &= \frac{2}{K(\psi^2-1)^{3/2}}\cdot\left[-\text{artanh}\beta+\psi\frac{\beta}{1-\beta^2}\right]\end{aligned}$$

Using the identity

$$\sinh(2\text{artanh}x) = \frac{(1+x)^2-(1-x)^2}{2(1-x^2)} = \frac{2x}{1-x^2}$$

$$\boxed{\delta s = \frac{1}{K(\psi^2-1)^{3/2}}\cdot[-2\text{artanh}\beta+\psi\sinh(2\text{artanh}\beta)]} \tag{124}$$

*****

Finally:

$$\delta s(\psi,\alpha_h) = \begin{cases}\dfrac{1}{K(1-\psi^2)^{3/2}}\cdot[2\arctan\beta-\psi\sin(2\arctan\beta)] & \text{if } \psi<1 \\ \dfrac{1}{K(\psi^2-1)^{3/2}}\cdot[-2\text{artanh}\beta+\psi\sinh(2\text{artanh}\beta)] & \text{if } \psi>1\end{cases} \tag{125}$$

with

$$\boxed{\begin{cases}K(\psi,\alpha_h) = \dfrac{C}{1+\psi\cos\alpha_h} \\ \beta(\psi,\alpha_h) = \sqrt{\left|\dfrac{1-\psi}{1+\psi}\right|}\cdot\tan\dfrac{\alpha_h}{2}\end{cases}} \tag{126}$$

One can check that $\delta s(\psi,\alpha_h)$ is continuous and differentiable as ψ goes to 1 and:

$$[K\delta s](\psi=1,\alpha_h) = \frac{\tan\frac{\alpha_h}{2}}{2}\cdot\left(1+\frac{\tan^2\frac{\alpha_h}{2}}{3}\right) \tag{127}$$

$$d[K\delta s](\psi=1,\alpha_h) = \frac{\tan\frac{\alpha_h}{2}}{2}\left(\frac{\tan^4\frac{\alpha_h}{2}}{5}-1\right)\cdot d\psi + \frac{1}{(1+\cos\alpha_h)^2}\cdot d\alpha_h \tag{128}$$

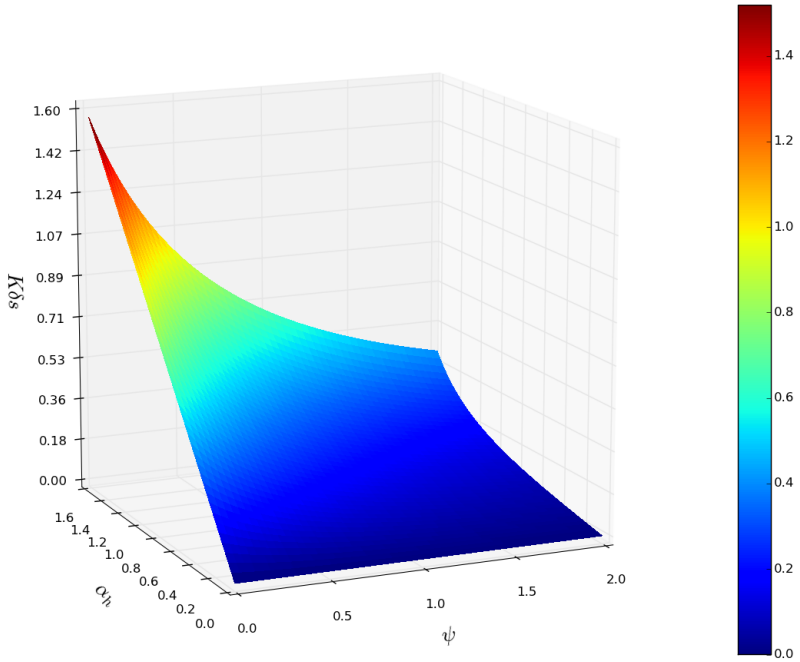

Figure 15: *$K\delta s$ as a function of ψ and α_h.*